Helicopter Tail Rotor Noise Analyses

Albert R. George and S.-T. Chou

Sibley School of
Mechanical and Aeorspace Engineering
Upson and Grumman Halls
Cornell University
Ithaca, New York 14853

Final Technical Report

Prepared for Langley Research Center
under Grant NAG -1-590
Period : June 1, 1985 - January 31, 1986

Summary

A study was made of helicopter tail rotor noise, particularly that due to interactions with the main rotor tip vortices, and with the fuselage separation mean wake.

The tail rotor blade - main rotor tip vortex interaction is modelled as an airfoil of infinite span cutting through a moving vortex. The vortex and the geometry information required by the analyses are obtained through a free wake geometry analysis of the main rotor. The acoustic pressure-time histories for the tail rotor blade-vortex interactions are then calculated. These acoustic results are compared to tail rotor loading and thickness noise, and are found to be significant to the overall tail rotor noise generation. Under most helicopter operating conditions, large acoustic pressure fluctuations can be generated due to a series of skewed main rotor tip vortices passing through the tail rotor disk. This noise generation depends strongly upon the helicopter operating conditions and the location of the tail rotor relative to the main rotor.

The interaction between the tail rotor and the fuselage separation mean wake does affect the loading noise characteristics, however it does not seem to be as important as the other harmonic noise sources such as thickness noise and blade-vortex interaction noise. However, the fuselage separation wake turbulence is important to tail rotor broadband noise.

Main Rotor Tip Vortex-Tail Rotor Interaction

During the forward flight of helicopters, tail rotors operate in a very complicated environment containing the main rotor wake, the fuselage wake, etc.[1] In this section, we will focus particularly on the tail rotor chopping the tip vortex convecting from the main rotor. The strong and concentrated main rotor tip vortex can generate significant velocity perturbations in the inflow field of the tail rotor. Using thin airfoil theory, these strong velocity perturbations can result in large unsteady loadings on the tail rotor blades; significant noise is therefore generated. In order to study the problem, clearly we first have to define the main rotor tip vortex trajectory around the tail rotor disk during flight conditions of interest.

Main Rotor Tip Vortex Free Wake Geometry Calculation

Since the main rotor tip vortex system is generally highly distorted, classical rigid wake analysis cannot predict the accurate trajectories of the vortex. The calculation of the free wake geometry of main rotor tip vortex is very important because the trajectories of vortex directly affect the characteristics of the interaction and the noise generated. In the present study, we use the comprehensive rotorcraft aerodynamics and dynamics analyses program (CAMRAD) of Johnson[2] to calculate the main rotor tip vortex wake geometry. The CAMRAD analysis is based on a rotor - free wake goemetry calculation model of Scully[3].

In our application, we assume non-uniform inflow at the main rotor disk, but the presence of the tail rotor is assumed to have no effect on the main rotor tip vortex system, and no fuselage wake effect is included. To demonstrate the analysis procedure, the UH-1D was selected to be the model helicopter for the present study. Three cases were run, which corresponding to a UH-1D at 100, 80, and 60 knots level flight respectively. Free wake geometry results are

presented in figures 1 through 3. From these results, the interactions between the tail rotor blade and the main rotor tip vortex are evident.

Determining the Locations of Blade-Vortex Interactions

The characteristics of a certain blade-vortex interaction are mainly determined by its location on the tail rotor blade. The normal incident velocity of the ingesting vortex relative to the tail rotor blade, the strength of the ingesting vortex element, and the skew angle between the ingesting vortex element and a line parallel to the rotor axis are the main controlling parameters for the tail rotor blade-main rotor tip vortex interaction noise. These parameters are generally not constant as a vortex sweeps through the tail rotor disk. Figures 4 through 6 present the main rotor tip vortex trajectories on the tail rotor disk, they correspond to the three cases shown in figures 1-3; the points shown are interpolated from the free wake geometry analysis results, and each point is exactly 15 degrees (main rotor rotation) apart.

Notice that the tip vortices involving in the interactions with the tail rotor are relatively "young" (less than 180° for all three cases considered), which implies that the ingested vortices are not fully rolled-up (Johnson[2] had suggested that a vortex is not fully rolled-up unless the vortex age is larger than 180° or so). Since a vortex is not fully rolled-up, the strength of the ingesting vortex should be less than the maximum bound circulation on the main rotor blade; we followed the assumption made by Scully[3], and set the strength of the tip vortex strength to 0.8 of the maximum bound circulation on the main rotor blade span.

Also the tail rotor RPM is generally not an integer multiplier of the main rotor RPM; the location of the blade-vortex interaction is different for each main rotor revolution. In the present study, both # 1 blades of the main and the tail rotors are set such that

both blades will start from $\psi = 0^o$ initially. (Figure 7 shows the definitions of azimuthal angle for both the main and the tail rotors.) The exact locations of a series of blade-vortex interactions can then be determined numerically. These results are shown in tables 1-3, they provide the required input data for the aerodynamic and acoustic analyses and are used in the following sections. Sketch of blade-vortex interaction geometry and vortex orientation are shown in figure 8.

Noise Generation Due to Blade-Vortex Interaction

The tail rotor blade-vortex interaction is modelled as a flat plate of infinite span chopping through a moving skewed vortex using a method similar to that of Amiet[4]. The acoustic pressure-time behavior is related to the airfoil lift response for certain perturbation velocity field. According to Amiet, the far field pressure-time history is given by

$$p(t) = i\cdot(\pi c z \rho_0 U^2/2a_0\sigma^2)\int_{-\infty}^{\infty} k_x \cdot \tilde{\tilde{w}}(k_x,k_y)\cdot L(k_x,k_y,M) \cdot \exp(i(k_x Ut+\mu(Mx-\sigma)))\, dk_x$$

where ρ_0 is the density of the acoustic medium, c is the tail rotor blade chord, a_0 is the speed of sound, $M = U/a_0$, $\mu = k_x M/(1-M^2)$, and $\sigma = \sqrt{x^2+(1-M^2)(y^2+z^2)}$. L is the effective lift function; see reference 4 for details. $\tilde{\tilde{w}}$ is the Fourier decomposed vortex velocity field.

In the present study, the effect of a moving vortex is included numerically, so U is the vortex normal velocity relative to the blade. Also in order to be consistent with the free wake geometry

analysis, a different vortex model is used. In the present analysis, the tangential velocity for a concentrated vortex is defined by the widely used model:

$$V_\theta = (\Gamma/2\pi r)\cdot r^2/(r^2+r_c^2)$$

where Γ is the vortex strength, r_c is the vortex core radius (r_c equals to 0.0025 of the main rotor tip radius in the present study). The vortex model Amiet used is given by

$$V_\theta = (\Gamma/2\pi r)\cdot(1+1/2\alpha)\cdot(1-\exp(-\alpha(r/r_c)^2)$$

where $\alpha = 1.25643$. At large radial location, the vortex model used in the present study decays more slowly than the model used by Amiet. Figure 9 shows the comparison between the two vortex models. Since a different vortex model is used, $\tilde{\tilde{w}}$, the Fourier decomposed vortex velocity which is normal to the tail rotor plane, is replaced by

$$\tilde{\tilde{w}} = i\cdot\tan\theta_v\Gamma r_c k_y K_1(r_c\sqrt{k_y^2+k_x^2/\cos^2\theta_v})/((2\pi)^2\sqrt{k_y^2+k_x^2/\cos^2\theta_v})$$

where K_1 is the modified Bessel function of the second kind, θ_v is defined in figure 8. It should be noted that $\tilde{\tilde{w}}$ only accounts for the effect of the tangential velocity of the vortices; the axial flow in the main rotor tip vortices is neglected in the present analysis as discussed in the conclusion.

To evaluate the effect of using the present vortex model, the acoustic pressure-time history for a given blade-vortex interaction is compared to that obtained using Amiet's original analysis. The comparison is shown in figure 10. Beside minor differences, the two

different analyses show very similar pressure-time behavior.

The data defining a series of blade-vortex interactions which we had obtained in the previous section are now used as the input for the noise calculation. Figure 11 shows the pressure-time history results for the tail rotor blade-main rotor tip vortex interaction of a UH-1D helicopter for 100 knots level flight (horizontal tick marks are 0.1 second apart); the far field observer is assumed to be stationary relative to the helicopter (the helicopter is positioned 50 m above the observer , and 25 m to the right of the observer). Notice that the pressure peaks are not separated by equal time intervals; therefore if one Fourier analyzed the pressure-time history, the resulting acoustic spectrum will behave more like broadband noise with widened spectrum peaks rather than pure harmonics. Figure 12, with a smaller time scale (horizontal tick marks are 0.01 second apart), shows the first 0.2 seconds of figure 11, showing the detailed shapes of the pressure peaks resulting from tail rotor blade-vortex interactions. Clearly an interaction with large normal velocity will result in a large but relatively short perturbation pressure peak; while an interaction characterized by smaller normal velocity will result in a lower but longer pressure perturbation.

Figures 13 and 14 show the similar results for a UH-1D at 80 knots level flight. Figures 15 and 16 show the acoustic results corresponding to the 60 knots level flight cases.

Effect of Tail Rotor Location

As discussed previously, the vortex trajectory on the tail rotor disk is very important to the tail rotor blade-vortex interaction noise. The tail rotor location relative to the main rotor, and the helicopter operating conditions are two primary variables that change the vortex trajectories on tail rotor disk. To study the effect of tail rotor location on the blade-vortex interaction noise, we

artificially lowered the UH-1D tail rotor by 0.5 m. This will cause the blade-vortex interactions to occur with advancing blades, thus enhancing the strength of the interactions.

For the 100 knots level flight case, the main rotor tip vortex trajectory on the tail rotor disk is now shown in figure 17. Notice that the path is higher than that shown in figure 4 due to a lowered tail rotor. As before, the interaction locations and vortex properties are then determined; results are shown in table 4. The acoustic pressure-history of the tail rotor blade-vortex interaction is shown in figure 18. There are considerable differences between the results shown in figures 10 and 18. Since the vortex is passing through the advancing side of the tail rotor, this results a higher relative velocity between the tail rotor blade and the vortex element, so generally the pressure perturbation has higher peaks. Also the interactions are more frequent than previous cases. Unquestionably, with this configuration (with lowered tail rotor), tail rotor noise will be higher than that from a standard tail rotor. Figure 19 shows the first 0.2 seconds of figure 18, showing the detailed pressure peak shape.

The 80 knots flight case is also studied; the tail rotor is also lowered by 0.5 m as in the previous case. The tip vortex trajectory is shown in figure 20. The input data to the acoustic analyses are given in table 5. The acoustic results are shown in figures 21 and 22. Again the results show higher pressure peaks and more frequent interactions.

Comparison to Other Noise Mechanisms

The tail rotor blade-vortex interaction noise is compared to other tail rotor noise sources in order to determine its relative importance to the overall helicopter noise radiation. We compare the noise generated by tail rotor blade-vortex interaction to the thickness noise and the steady loading noise. The thickness and

loading noises are calculated using program WOPWOP of Langley, the calculations are based on the analysis of Farassat[5]. Tail rotor loading is calculated using approximate aerodynamic analysis, and the loading is matched to balance the main rotor torque calculated in the free wake geometry analysis.

Only one case is presented, this is for a standard tail rotor at 100 knots level flight. Figures 23-26 plot the first four tail rotor blade-main rotor tip vortex interaction signals (see figure 11) along with the calculated thickness and loading noise results. Each figure shows the pressure-time history representing one tail rotor revolution; the solid line shows the overall thickness and loading noise, and the dash line shows the tail rotor blade-vortex interaction signal.

Notice that these figures do not include some of the strongest peaks, and they do not represent four consecutive tail rotor revolutions. For cases such as a 100 knots UH-1D with lowered tail rotor, the result not presented here show stronger tail rotor blade-vortex interaction peaks. However, even in the case shown, the importance of the tail rotor blade - main rotor tip vortex interaction is quite evident.

Tail Rotor - Fuselage Separation Wake Interaction

The effect of the fuselage separation mean wake on tail rotor noise is also studied. The separation mean wake is modelled as an axially-symmetric wake, and the wake is assumed to be steady. This will primarily affect the loading noise as the tail rotor inflow is changed. We scaled the BK-117 fuselage separation wake results of Polz and Quentin[6], and use them to calculate the resulting loading noise. The fuselage separation mean wake for an 80 knots level flight BK-117 is expressed by the velocity deficit U_d:

$$U_d = 0.7\ U_h\ \exp(-(z+1.15)/0.8656)$$

where U_h is the helicopter flight speed, and the definition of z is shown in figure 8.

The results are shown in figures 27 and 28; figure 27 gives the acoustic pressure-time history for 180° of the tail rotor rotation, and figure 28 shows the acoustic pressure spectrum obtained from the pressure-time history results shown in figure 27. In figure 27, the solid line shows the overall noise, the dash line shows thickness noise, and the dotted line shows the loading noise. In figure 28, the 'o' symbols show the overall harmonic noise level, the '+' symbols represent the thickness noise, and the '*' symbols represent the loading noise. Figures 29 and 30 show similar results for the BK-117 in 80 knots level flight except that no fuselage separation wake effect is included. Both of the two cases are for an observer fixed in space, and the BK-117 is 50 m above the observer and 25 m to the right of the observer. Notice that the pressure-time histories shown in figures 27 and 29 are not periodic, this is due to the fact that the observer is not moving with the helicopter.

In this particular case, the loading noise is much smaller than the thickness noise, and the fuselage separation wake does not result

in any significant change to the overall tail rotor noise. Since the presence of the fuselage separation mean wake generally does not result in any unsteady loading fluctuation of significant amplitude on the tail rotor blade, it will not be very significant to the tail rotor noise. However, the fuselage separation wake turbulence will have an important effect on the high-frequency tail rotor broadband noise[1].

Conclusions

Tail rotor blade-main rotor tip vortex interaction is a very important tail rotor noise mechanism. The noise generated depends strongly on the main rotor operating conditions and on the tail rotor location. Major parameters governing this blade-vortex noise generation are the ingested vortex strength, the ingested vortex skew angle relative to the blade, and the relative velocity of the ingested vortex to the tail rotor blade. The present study shows that this noise mechanism is at least of the same order of magnitude as some of the strongest tail rotor noise sources such as thickness noise. More detailed study should be devoted to the problem considering a vortex chopped by an airfoil of finite span.

The present study does not include the possibly major effect of the axial flow in the main rotor tip vortex. This can be another strong contributor to the unsteady loading fluctuation on a tail rotor blade. The result of free wake geometry analysis does indicate some evidence of the main rotor tip vortex drifting normal to the tail rotor disk. Also the strength of main rotor tip vortex is not constant, this will result in an axial pressure gradient inside the vortex, thus inducing some axial flow. These important problems should be addressed in future studies.

The fuselage separation mean wake effect does not seem to be as important as the tail rotor blade-vortex interaction noise. However, the fuselage turbulent wake, with small scale turbulent eddies, will be an important tail rotor broadband noise source when it is ingested into the tail rotor disk.

Reference

1. George, A. R., Chou, S.-T.: A Comparative Study of Tail Rotor Noise Mechanisms. Proceedings of the American Helicopter Society 41st Annual Forum, Fort Worth, Texas, May 1985.

2. Scully, M. P.: Computation of Helicopter Rotor Wake Geometry and its Influence on Rotor Harmonic Airloads. M.I.T. ASRL Report TR 178-1, March, 1975.

3. Johnson, W.: A Comprehensive Analytical Model of Rotorcraft Aerodynamics and Dynamics, Part I, II, and III. NASA TM 81182, 81183, and 81184, 1980.

4. Schlinker, R. H., Amiet, R. K.: Rotor-Vortex Interaction Noise. NASA CR 3744, October 1983.

5. Farassat, F., Succi, G. P.: The Prediction of Helicopter Rotor Discrete Frequency Noise. Vertica, Vol. 7, No. 4, 1983.

6. Polz, G., Quentin, J.: Separated Flow Around Helicopter Bodies. Paper # 48, 7th European Rotorcraft and Powered Lift Aircraft Forum, September, 1981.

TABLE 1. TAIL ROTOR BLADE-VORTEX INTERACTION
UH-1D 100 KNOTS, STANDARD TAIL ROTOR

M.R. PSI	RADIUS	T.R. PSI	U	THETAV	PHIV	GAMMA	T.R. #
32.976	0.721	168.753	123.087	19.181	-84.670	11.855	1
102.534	1.204	345.368	207.403	19.411	-252.082	11.791	2
208.537	0.843	168.410	144.768	19.177	-84.847	11.859	2
278.145	1.083	345.151	186.263	19.381	-252.554	11.795	1
384.161	0.964	168.167	166.026	19.187	-85.039	11.863	1
453.756	0.961	344.880	165.075	19.352	-252.972	11.799	2
559.786	1.085	167.977	187.235	19.196	-85.286	11.868	2
629.359	0.840	344.544	143.791	19.323	-253.307	11.804	1
735.410	1.206	167.826	208.411	19.206	-85.570	11.872	1
804.913	0.717	344.192	122.254	19.306	-253.514	11.807	2
980.467	0.595	343.695	100.586	19.288	-253.576	11.811	1
1122.367	0.461	170.102	76.629	19.204	-84.838	11.846	2
1156.021	0.472	342.940	78.690	19.270	-253.380	11.815	2
1297.897	0.584	169.311	98.877	19.193	-84.608	11.850	1
1327.379	0.234	339.286	33.904	19.238	-250.793	11.823	1
1473.427	0.708	168.796	120.879	19.182	-84.655	11.855	2
1542.976	1.216	345.387	209.530	19.414	-252.032	11.791	1
1648.978	0.831	168.439	142.623	19.176	-84.832	11.859	1
1718.587	1.095	345.175	188.395	19.384	-252.509	11.795	2
1824.602	0.952	168.188	163.887	19.186	-85.017	11.863	2
1894.198	0.974	344.910	167.212	19.355	-252.933	11.799	1
2000.226	1.073	167.994	185.100	19.195	-85.259	11.867	1
2069.807	0.853	344.574	145.956	19.325	-253.280	11.803	2
2175.851	1.194	167.840	206.278	19.205	-85.540	11.871	2
2245.361	0.730	344.233	124.428	19.307	-253.499	11.807	1
2420.915	0.607	343.754	102.778	19.290	-253.579	11.811	2
2562.818	0.448	170.206	74.366	19.206	-84.885	11.845	1
2596.469	0.485	343.033	80.910	19.272	-253.417	11.815	1
2738.347	0.572	169.375	96.649	19.195	-84.616	11.850	2
2768.376	0.261	340.046	39.373	19.242	-251.430	11.822	2

TABLE 2. TAIL ROTOR BLADE-VORTEX INTERACTION
UH-1D 80 KNOTS, STANDARD TAIL ROTOR

M.R. PSI	RADIUS	T.R. PSI	U	THETAV	PHIV	GAMMA	T.R. #
33.294	0.879	170.351	147.861	17.005	-87.191	13.130	1
100.352	0.623	334.907	100.834	17.369	-243.453	13.089	2
208.790	0.979	169.670	165.672	16.992	-87.003	13.133	2
275.577	0.519	332.906	81.472	17.330	-242.187	13.092	1
384.363	1.077	169.134	183.107	16.971	-86.833	13.135	1
450.802	0.416	329.911	61.558	17.292	-239.929	13.095	2
487.928	1.226	339.974	209.299	17.587	-245.345	13.073	1
559.936	1.175	168.687	200.487	16.949	-86.752	13.138	2
597.642	0.347	180.723	47.814	17.096	-94.612	13.115	1
620.508	0.202	313.943	13.551	17.217	-225.215	13.101	1
663.508	1.129	339.530	192.078	17.550	-245.355	13.076	2
735.509	1.273	168.310	217.828	16.927	-86.741	13.141	1
772.621	0.455	176.631	69.526	17.070	-91.138	13.118	2
839.072	1.032	338.996	174.753	17.514	-245.284	13.078	1
947.600	0.564	174.115	90.367	17.044	-89.239	13.121	1
1014.572	0.933	338.328	157.152	17.480	-245.109	13.081	2
1122.815	0.669	172.472	109.809	17.025	-88.177	13.124	2
1190.073	0.835	337.502	139.461	17.446	-244.776	13.083	1
1298.282	0.769	171.318	128.007	17.016	-87.563	13.127	1
1365.573	0.737	336.456	121.646	17.411	-244.223	13.086	2
1473.750	0.869	170.429	146.049	17.006	-87.215	13.130	2
1540.833	0.633	335.072	102.763	17.373	-243.544	13.089	1
1649.236	0.969	169.729	163.913	16.994	-87.026	13.132	1
1716.058	0.529	333.143	83.443	17.334	-242.350	13.091	2
1824.809	1.067	169.183	181.352	16.973	-86.845	13.135	2
1891.283	0.426	330.278	63.599	17.295	-240.221	13.094	1
1928.373	1.236	340.015	211.033	17.591	-245.340	13.073	2
2000.382	1.165	168.729	198.739	16.951	-86.757	13.138	1
2038.148	0.337	181.280	45.548	17.098	-95.107	13.114	2
2061.657	0.225	317.196	19.584	17.225	-228.331	13.100	2
2103.953	1.139	339.578	193.814	17.554	-245.357	13.076	1
2175.955	1.263	168.345	216.082	16.930	-86.739	13.140	2
2213.127	0.444	176.953	67.389	17.072	-91.398	13.118	1
2279.525	1.042	339.057	176.522	17.517	-245.295	13.078	2
2388.106	0.553	174.324	88.292	17.046	-89.386	13.121	2
2455.025	0.943	338.402	158.928	17.483	-245.133	13.081	1
2563.271	0.659	172.608	107.966	17.026	-88.258	13.124	1
2630.526	0.845	337.594	141.248	17.449	-244.819	13.083	2
2738.739	0.759	171.421	126.181	17.017	-87.611	13.127	2
2806.027	0.746	336.574	123.447	17.415	-244.292	13.085	1

TABLE 3. TAIL ROTOR BLADE-VORTEX INTERACTION
UH-1D 60 KNOTS, STANDARD TAIL ROTOR

M.R. PSI	RADIUS	T.R. PSI	U	THETAV	PHIV	GAMMA	T.R. #
33.357	1.050	170.768	176.808	14.661	-88.140	14.893	1
71.558	0.439	185.614	62.689	14.910	-98.775	14.881	2
133.915	0.652	326.332	104.390	15.432	-232.263	14.861	1
170.623	1.244	334.253	211.438	15.817	-236.717	14.851	2
208.873	1.123	170.099	189.981	14.633	-87.939	14.894	2
246.486	0.517	181.651	78.221	14.879	-95.330	14.882	1
309.010	0.575	324.076	89.799	15.385	-230.486	14.863	2
346.191	1.172	333.722	198.611	15.771	-236.562	14.852	1
384.434	1.196	169.527	202.953	14.606	-87.646	14.896	1
421.414	0.596	178.733	93.563	14.848	-92.930	14.884	2
484.106	0.499	321.127	75.065	15.337	-228.015	14.865	1
521.721	1.099	333.116	185.662	15.726	-236.377	14.853	2
559.995	1.269	169.020	215.906	14.579	-87.419	14.897	2
596.656	0.672	176.628	107.831	14.815	-91.338	14.885	1
658.938	0.421	316.887	59.347	15.288	-224.282	14.866	2
697.238	1.027	332.422	172.651	15.680	-236.120	14.855	1
772.020	0.746	174.988	121.646	14.782	-90.210	14.887	2
832.414	0.328	308.754	39.202	15.233	-216.802	14.868	1
872.754	0.954	331.622	159.614	15.634	-235.758	14.856	2
947.383	0.821	173.647	135.392	14.749	-89.380	14.888	1
1005.889	0.246	294.740	19.088	15.178	-203.441	14.870	2
1048.228	0.881	330.681	146.422	15.587	-235.254	14.857	1
1122.812	0.895	172.546	148.911	14.719	-88.801	14.890	2
1166.382	0.239	211.348	16.823	15.008	-122.955	14.876	1
1223.634	0.807	329.553	132.997	15.537	-234.560	14.859	2
1298.312	0.969	171.629	162.209	14.691	-88.415	14.891	1
1338.377	0.340	193.709	41.516	14.954	-106.161	14.879	2
1399.040	0.734	328.198	119.516	15.487	-233.640	14.860	1
1473.811	1.042	170.841	175.473	14.663	-88.160	14.893	2
1512.068	0.431	186.092	61.113	14.913	-99.200	14.881	1
1574.409	0.660	326.530	105.853	15.437	-232.413	14.861	2
1611.069	1.251	334.303	212.728	15.822	-236.729	14.850	1
1649.319	1.116	170.161	188.674	14.636	-87.973	14.894	1
1686.997	0.509	181.996	76.666	14.882	-95.622	14.882	2
1749.504	0.583	324.330	91.274	15.390	-230.692	14.863	1
1786.637	1.179	333.779	199.904	15.776	-236.581	14.852	2
1824.881	1.189	169.581	201.647	14.609	-87.672	14.896	2
1861.925	0.588	178.992	92.025	14.851	-93.136	14.883	1
1924.600	0.507	321.464	76.558	15.342	-228.304	14.864	2
1962.173	1.107	333.181	186.971	15.730	-236.398	14.853	1
2000.442	1.262	169.068	214.602	14.581	-87.439	14.897	1
2037.123	0.664	176.813	106.435	14.818	-91.472	14.885	2
2099.595	0.431	317.508	61.354	15.294	-224.837	14.866	1
2137.690	1.034	332.496	173.963	15.684	-236.151	14.854	2
2212.487	0.738	175.139	120.258	14.785	-90.309	14.887	1
2273.071	0.337	309.775	41.247	15.239	-217.757	14.868	2
2313.206	0.961	331.708	160.928	15.639	-235.800	14.856	1

TABLE 3 - CONTINUED

M.R. PSI	RADIUS	T.R. PSI	U	THETAV	PHIV	GAMMA	T.R. #
2387.850	0.813	173.771	134.009	14.752	-89.453	14.888	2
2446.547	0.253	296.548	21.060	15.184	-205.183	14.870	1
2488.691	0.888	330.785	147.772	15.592	-235.314	14.857	2
2563.266	0.888	172.647	147.570	14.721	-88.848	14.890	1
2607.188	0.230	213.926	14.492	15.013	-125.449	14.876	2
2664.097	0.815	329.676	134.351	15.542	-234.639	14.859	1
2738.765	0.961	171.715	160.871	14.694	-88.448	14.891	2
2779.184	0.328	194.981	38.998	14.959	-107.348	14.879	1
2839.503	0.741	328.346	120.877	15.492	-233.745	14.860	2

TABLE 4. TAIL ROTOR BLADE-VORTEX INTERACTION
UH-1D 100 KNOTS, LOWERED TAIL ROTOR

M.R. PSI	RADIUS	T.R. PSI	U	THETAV	PHIV	GAMMA	T.R. #
27.565	1.088	141.595	211.687	19.179	-58.128	11.860	1
54.738	0.514	103.671	137.105	19.211	-16.784	11.835	2
77.516	0.605	35.597	145.656	19.276	54.150	11.814	1
106.904	1.293	7.534	243.277	19.439	86.363	11.787	2
203.616	1.188	143.810	227.163	19.188	-60.737	11.864	2
231.803	0.555	111.133	140.759	19.211	-24.635	11.837	1
254.330	0.551	42.526	140.332	19.264	46.822	11.817	2
282.956	1.192	9.339	227.257	19.414	84.013	11.791	1
379.666	1.289	145.679	243.174	19.197	-62.999	11.868	1
408.868	0.605	117.461	145.766	19.211	-31.352	11.840	2
431.630	0.513	49.473	137.039	19.254	39.544	11.819	1
459.111	1.094	11.425	212.171	19.388	81.323	11.794	2
585.934	0.661	122.772	152.056	19.211	-37.052	11.842	1
608.930	0.483	57.393	134.853	19.244	31.291	11.822	2
635.265	0.998	13.917	197.694	19.362	78.228	11.798	1
762.545	0.732	127.846	160.775	19.205	-42.559	11.845	2
786.230	0.464	66.146	133.630	19.234	22.206	11.824	1
811.420	0.904	16.930	183.992	19.336	74.610	11.802	2
938.945	0.812	132.233	171.451	19.196	-47.398	11.849	1
963.530	0.457	75.411	133.198	19.224	12.608	11.827	2
987.890	0.822	20.337	172.382	19.318	70.716	11.805	1
1115.344	0.897	135.812	183.281	19.187	-51.431	11.853	2
1140.830	0.462	84.734	133.465	19.214	2.953	11.829	1
1164.544	0.746	24.279	162.428	19.304	66.353	11.808	2
1291.744	0.984	138.767	196.028	19.178	-54.838	11.856	1
1317.968	0.479	94.139	134.580	19.211	-6.823	11.832	2
1341.198	0.676	29.074	153.657	19.291	61.137	11.811	1
1467.963	1.078	141.349	210.162	19.178	-57.842	11.860	2
1495.033	0.510	102.855	136.811	19.211	-15.928	11.834	1
1517.853	0.611	34.938	146.309	19.277	54.852	11.814	2
1644.013	1.178	143.604	225.578	19.187	-60.491	11.864	1
1672.099	0.551	110.434	140.329	19.211	-23.897	11.837	2
1694.602	0.555	41.881	140.728	19.265	47.501	11.816	1
1723.344	1.202	9.148	228.806	19.417	84.265	11.791	2
1820.064	1.279	145.504	241.540	19.196	-62.784	11.867	2
1849.164	0.600	116.872	145.202	19.211	-30.724	11.839	1
1871.902	0.516	48.728	137.319	19.255	40.322	11.819	2
1899.498	1.104	11.199	213.665	19.391	81.611	11.794	1
2026.229	0.655	122.279	151.368	19.211	-36.520	11.842	2
2049.202	0.486	56.554	135.026	19.245	32.164	11.821	1
2075.653	1.008	13.644	199.121	19.364	78.561	11.798	2
2202.908	0.724	127.351	159.775	19.206	-42.018	11.845	1
2226.502	0.466	65.234	133.715	19.235	23.151	11.824	2
2251.807	0.914	16.599	185.331	19.338	75.003	11.801	1
2379.307	0.804	131.831	170.319	19.197	-46.951	11.849	2
2403.802	0.457	74.467	133.210	19.225	13.585	11.826	1
2428.227	0.829	19.980	173.442	19.319	71.115	11.805	2

TABLE 4 - CONTINUED

M.R. PSI	RADIUS	T.R. PSI	U	THETAV	PHIV	GAMMA	T.R. #
2555.707	0.888	135.482	182.044	19.188	-51.056	11.852	1
2581.102	0.461	83.806	133.406	19.215	3.914	11.829	2
2604.881	0.754	23.847	163.381	19.306	66.827	11.807	1
2732.106	0.975	138.493	194.708	19.179	-54.519	11.856	2
2758.263	0.477	93.204	134.420	19.211	-5.849	11.832	1
2781.535	0.683	28.546	154.481	19.292	61.707	11.810	2

TABLE 5. TAIL ROTOR BLADE-VORTEX INTERACTION
UH-1D 80 KNOTS, LOWERED TAIL ROTOR

M.R. PSI	RADIUS	T.R. PSI	U	THETAV	PHIV	GAMMA	T.R. #
28.302	1.186	145.116	220.053	16.990	-62.489	13.133	1
59.068	0.581	123.063	129.149	17.103	-36.777	13.114	2
82.624	0.388	61.452	109.593	17.232	27.528	13.099	1
108.368	0.759	14.507	153.067	17.433	78.032	13.084	2
204.195	1.273	146.431	234.210	16.970	-64.144	13.135	2
235.454	0.644	127.730	137.332	17.084	-41.888	13.116	1
259.907	0.380	70.367	109.103	17.212	18.290	13.101	2
284.602	0.688	17.892	142.883	17.404	74.216	13.086	1
411.841	0.710	131.545	146.498	17.066	-46.148	13.118	2
437.189	0.381	79.458	109.188	17.193	8.875	13.103	1
461.273	0.627	21.565	134.751	17.377	70.031	13.088	2
492.384	1.248	2.517	229.839	17.624	92.570	13.071	1
588.227	0.779	134.696	156.453	17.047	-49.743	13.121	1
614.421	0.392	88.440	109.880	17.174	-0.433	13.104	2
637.944	0.570	25.998	127.480	17.350	65.085	13.090	1
668.336	1.163	3.832	216.002	17.590	90.838	13.073	2
764.578	0.851	137.350	167.153	17.029	-52.845	13.123	2
791.443	0.413	97.347	111.466	17.161	-9.671	13.106	1
814.615	0.517	31.378	121.247	17.323	59.192	13.092	2
844.288	1.079	5.354	202.425	17.557	88.901	13.075	1
940.624	0.931	139.747	179.366	17.021	-55.713	13.126	1
968.466	0.444	105.197	114.060	17.147	-17.853	13.108	2
991.286	0.470	37.916	116.219	17.295	52.141	13.094	1
1020.240	0.996	7.132	189.172	17.523	86.706	13.078	2
1116.671	1.012	141.763	192.052	17.012	-58.200	13.128	2
1145.488	0.482	111.927	117.738	17.133	-24.915	13.110	1
1168.332	0.434	44.888	112.940	17.273	44.772	13.096	2
1196.402	0.918	9.100	176.989	17.494	84.320	13.080	1
1292.717	1.094	143.478	205.115	17.004	-60.387	13.130	1
1322.510	0.525	117.613	122.476	17.120	-30.932	13.111	2
1345.615	0.408	52.312	110.906	17.253	37.025	13.098	1
1372.577	0.841	11.419	165.293	17.465	81.581	13.082	2
1468.716	1.178	144.973	218.640	16.992	-62.312	13.133	2
1499.432	0.575	122.537	128.388	17.105	-36.206	13.113	1
1522.898	0.390	60.580	109.677	17.234	28.433	13.099	2
1548.753	0.766	14.197	154.153	17.436	78.384	13.084	1
1644.609	1.264	146.307	232.774	16.972	-63.985	13.135	1
1675.819	0.637	127.302	136.459	17.086	-41.415	13.116	2
1700.180	0.380	69.453	109.126	17.214	19.236	13.101	1
1724.938	0.694	17.558	143.744	17.406	74.602	13.086	2
1852.205	0.703	131.194	145.536	17.067	-45.752	13.118	1
1877.463	0.380	78.547	109.154	17.195	9.819	13.103	2
1901.608	0.633	21.164	135.534	17.379	70.484	13.088	1
1932.792	1.257	2.394	231.246	17.628	92.735	13.070	2
2028.591	0.772	134.404	155.419	17.049	-49.407	13.121	2
2054.721	0.390	87.494	109.770	17.176	0.547	13.104	1
2078.280	0.576	25.511	128.169	17.352	65.623	13.090	2

TABLE 5 - CONTINUED

M.R. PSI	RADIUS	T.R. PSI	U	THETAV	PHIV	GAMMA	T.R. #
2108.743	1.172	3.691	217.385	17.594	91.021	13.073	1
2204.976	0.843	137.084	165.953	17.030	-52.531	13.123	1
2231.744	0.411	96.495	111.263	17.162	-8.785	13.106	2
2254.950	0.522	30.787	121.823	17.325	59.835	13.092	1
2284.696	1.088	5.190	203.780	17.560	89.106	13.075	2
2381.022	0.923	139.524	178.112	17.021	-55.443	13.125	2
2408.766	0.441	104.457	113.750	17.148	-17.080	13.108	1
2431.621	0.474	37.199	116.667	17.298	52.910	13.094	2
2460.647	1.004	6.940	190.490	17.526	86.941	13.078	1
2557.069	1.004	141.574	190.755	17.013	-57.964	13.128	1
2585.788	0.478	111.298	117.318	17.135	-24.252	13.110	2
2608.606	0.437	44.192	113.194	17.275	45.501	13.096	1
2636.787	0.926	8.887	178.194	17.497	84.575	13.080	2
2733.115	1.086	143.317	203.784	17.005	-60.178	13.130	2
2762.810	0.521	117.083	121.953	17.121	-30.369	13.111	1
2785.889	0.410	51.523	111.073	17.255	37.846	13.097	2
2812.963	0.849	11.167	166.448	17.467	81.876	13.082	1

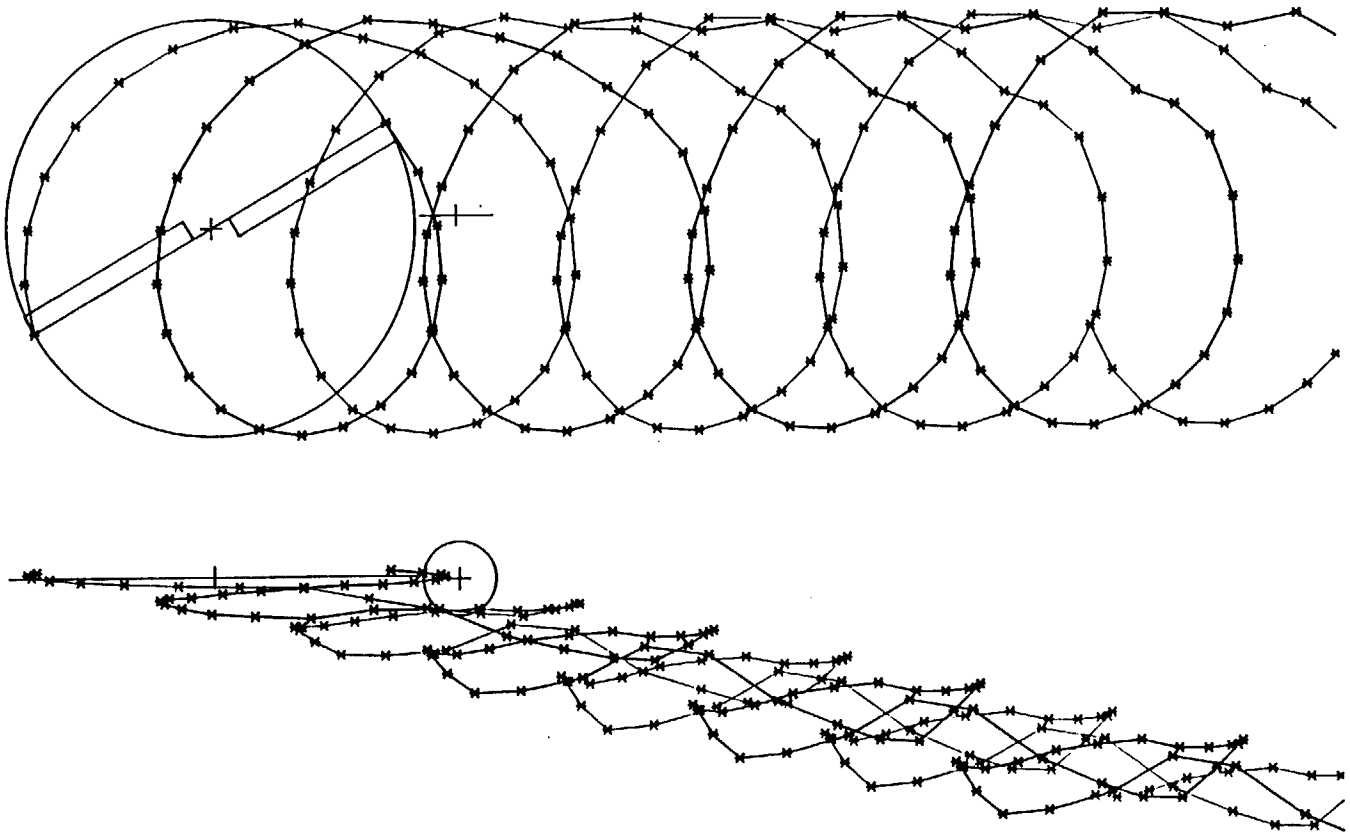

Figure 1 Free Wake Geometry Analysis Result

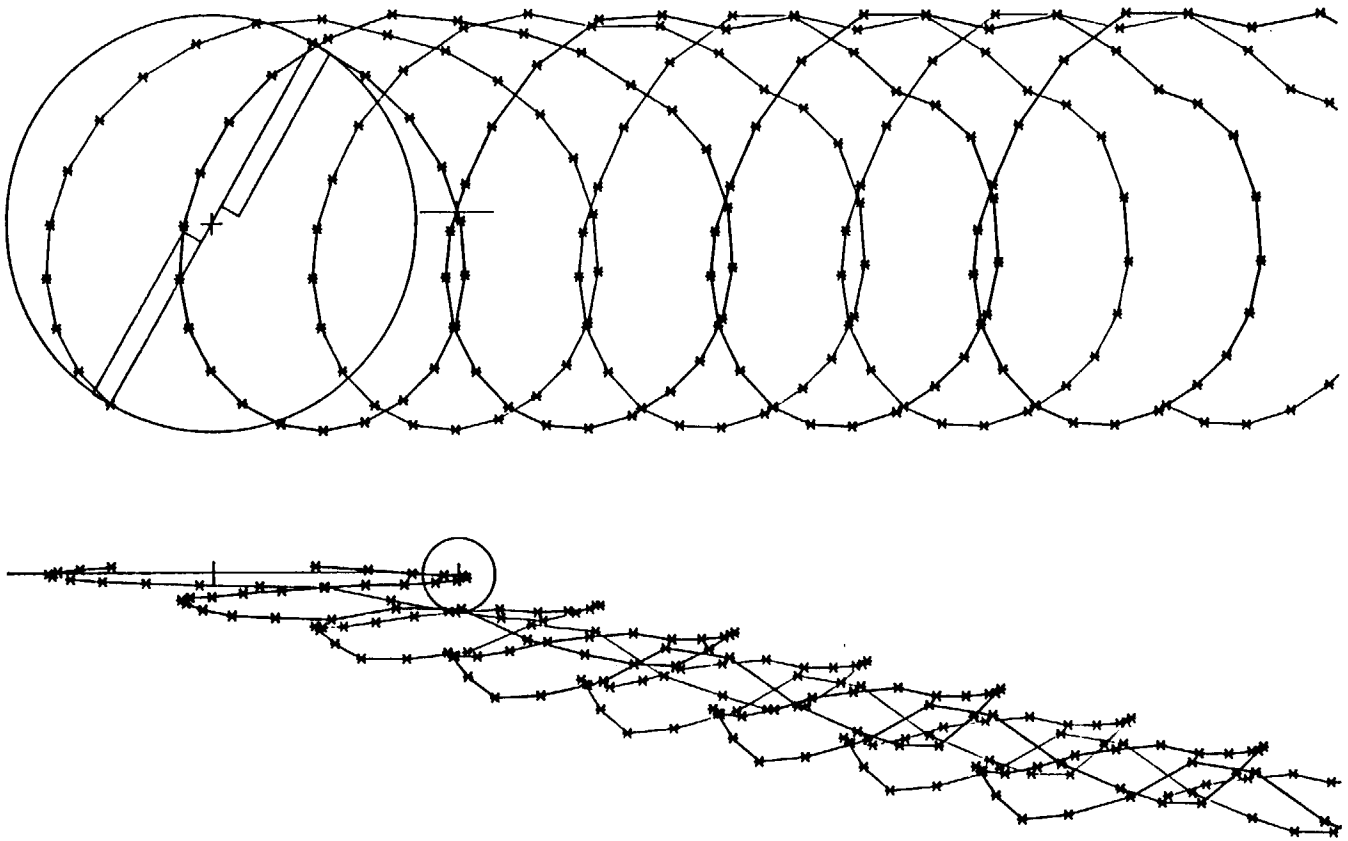

PSI = 60. DEGREES
UH-1D, 100.0 KNOTS

Figure 1 - Continued

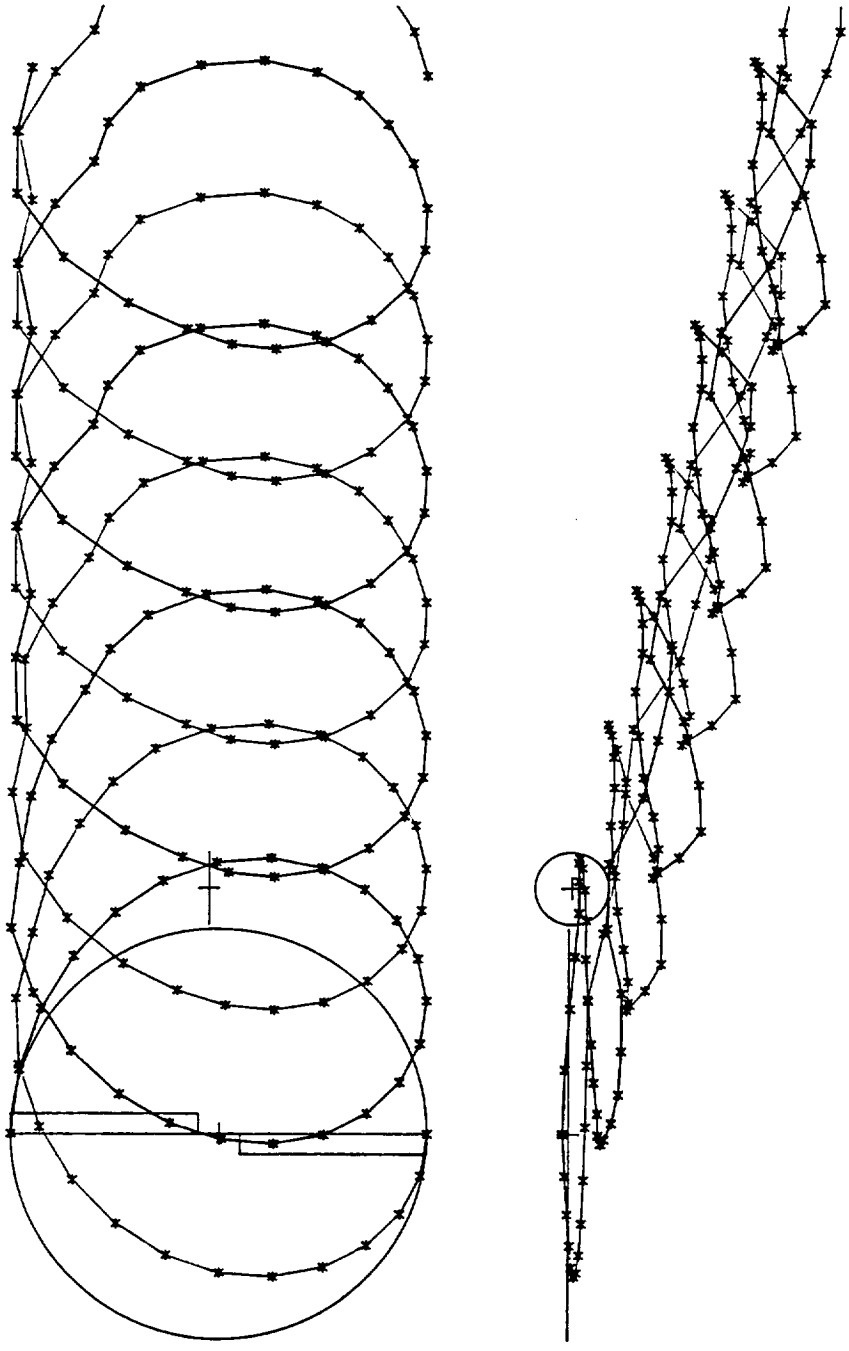

Figure 1 - Continued

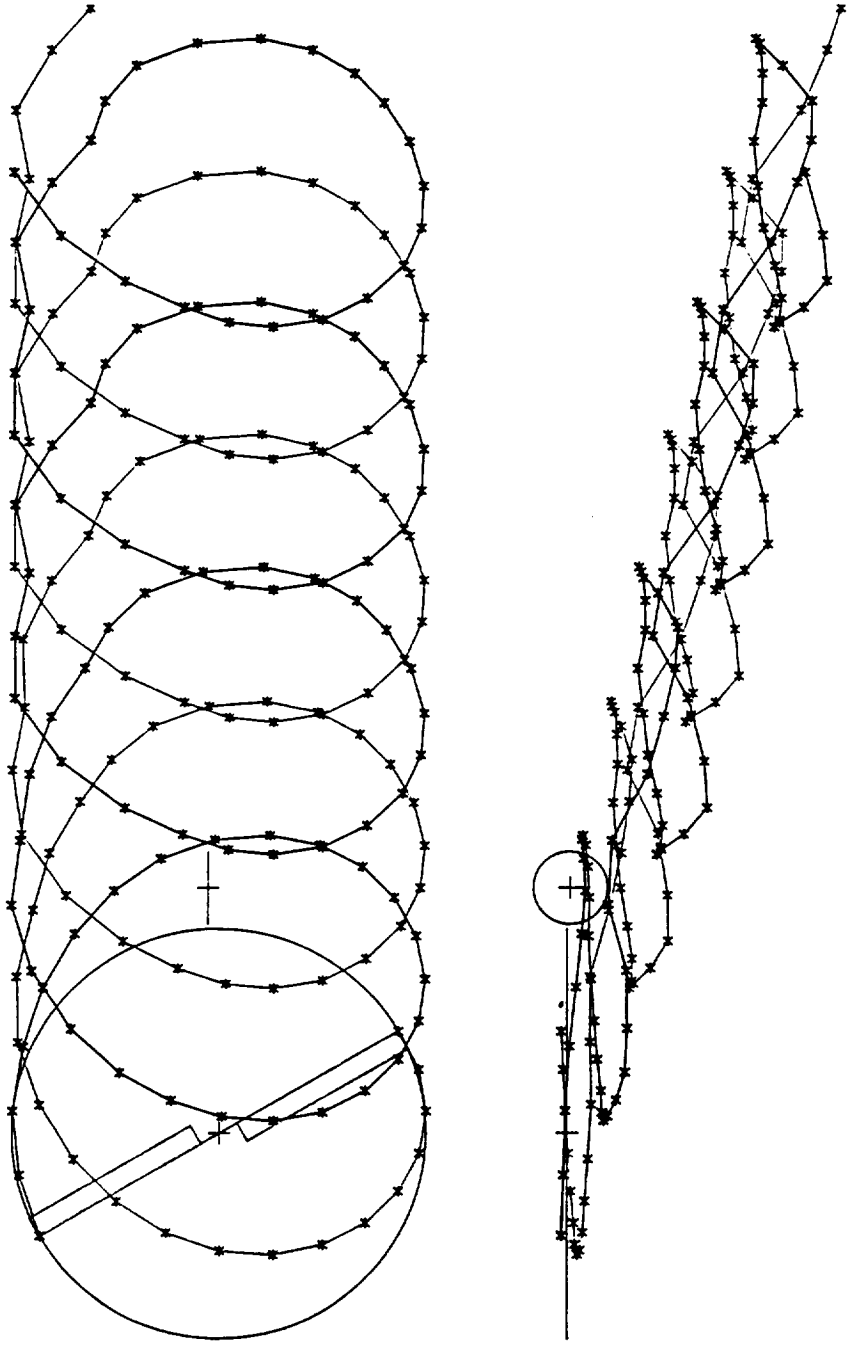

PSI = 120. DEGREES
UH-1D, 100.0 KNOTS

Figure 1 - Continued

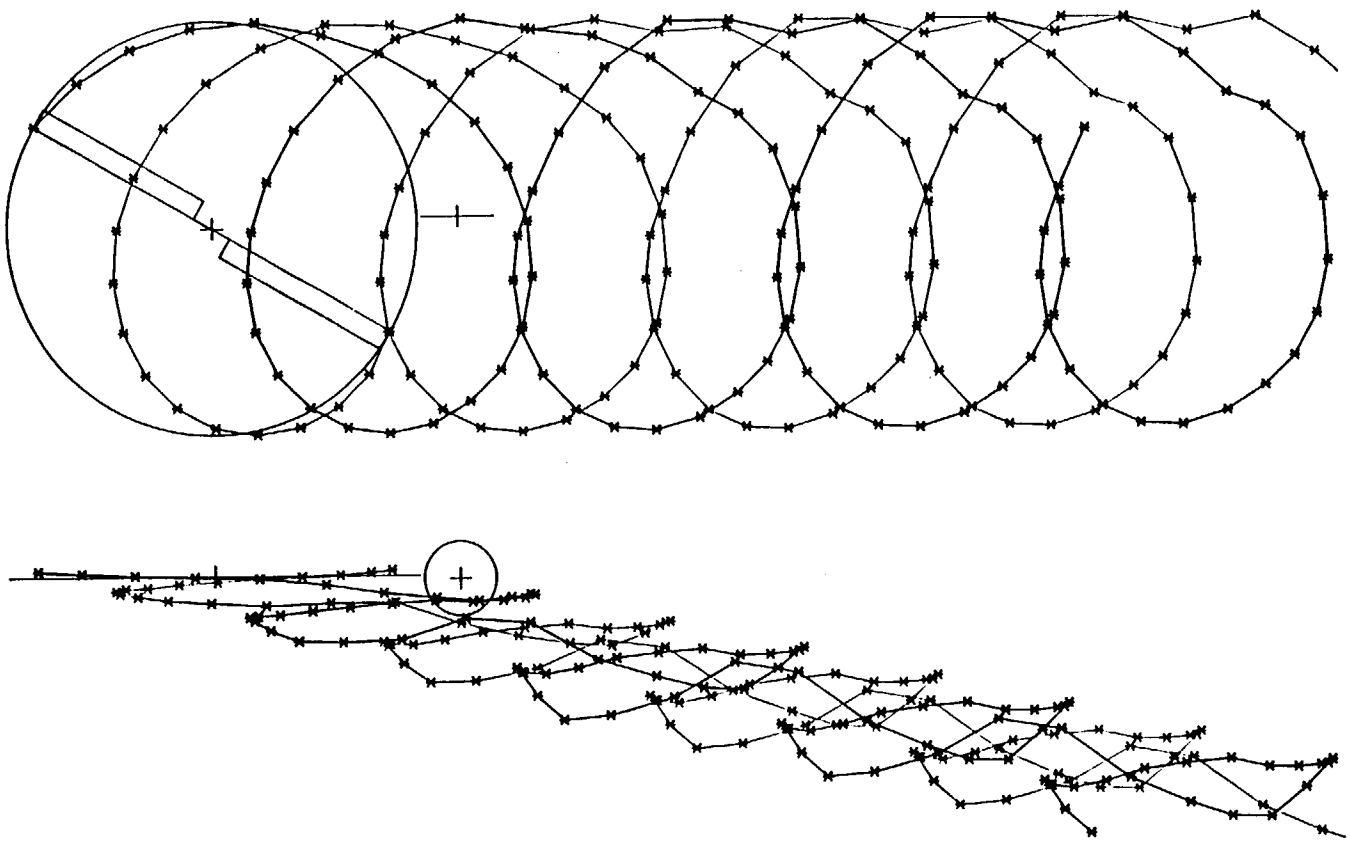

PSI = 150. DEGREES
UH-1D, 100.0 KNOTS

Figure 1 - Continued

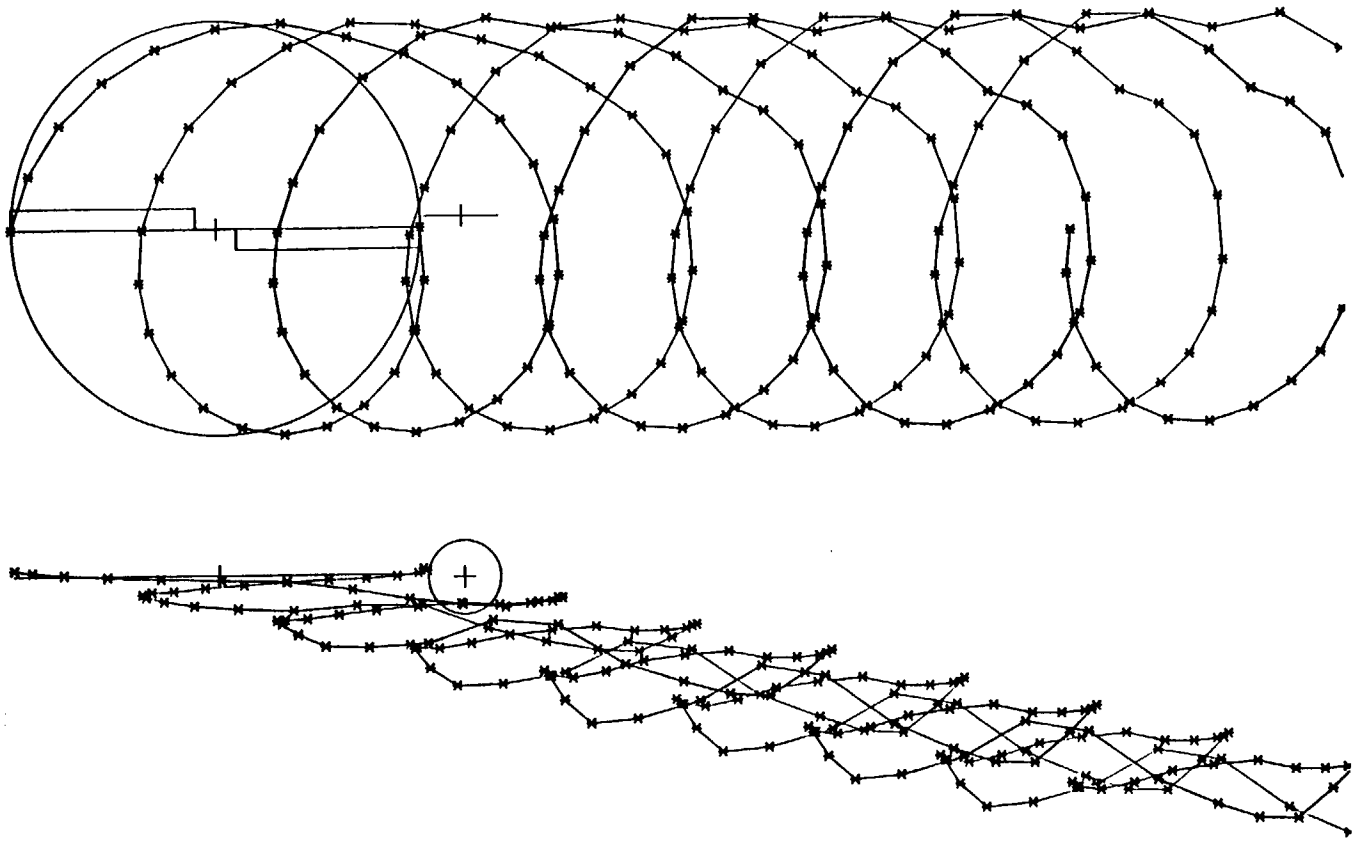

PSI = 180. DEGREES
UH-1D, 100.0 KNOTS

Figure 1 - Continued

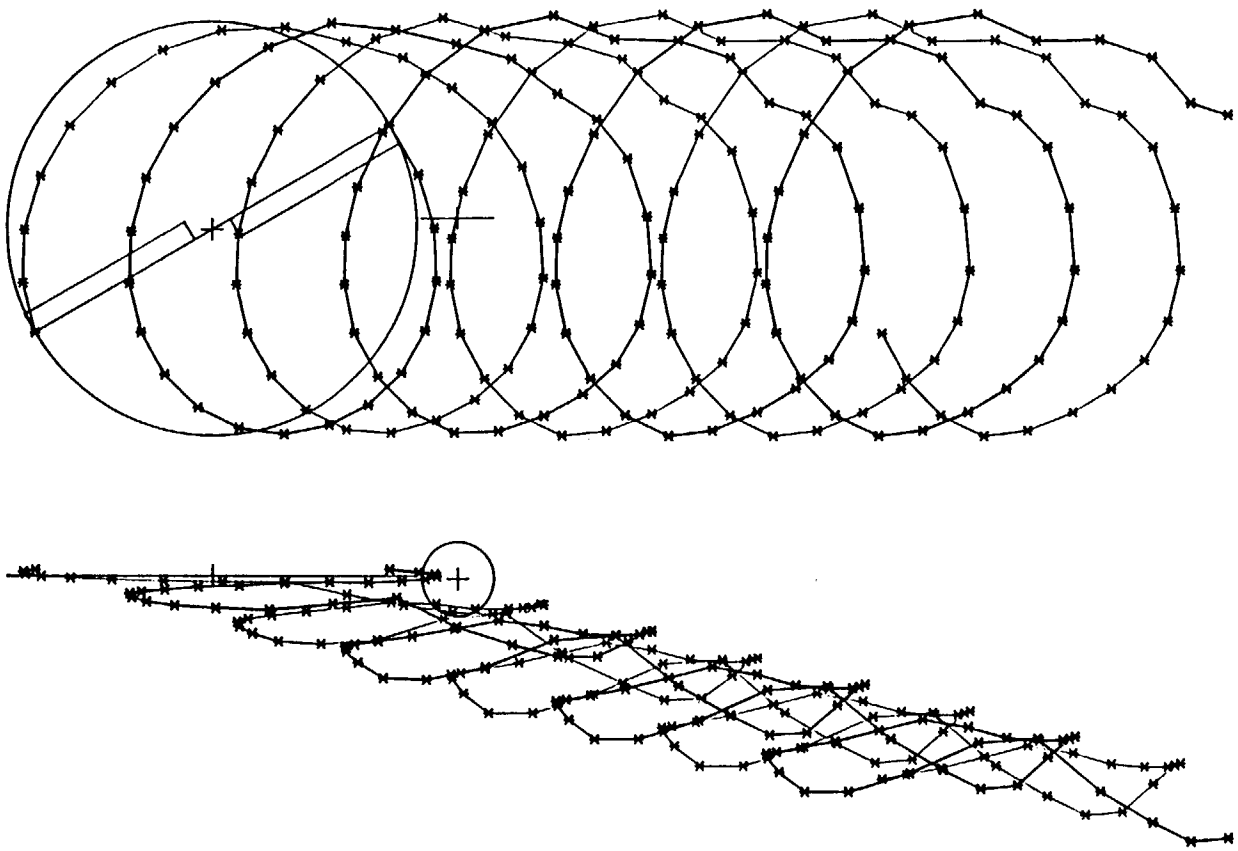

Figure 2 Free Wake Geometry Analysis Result

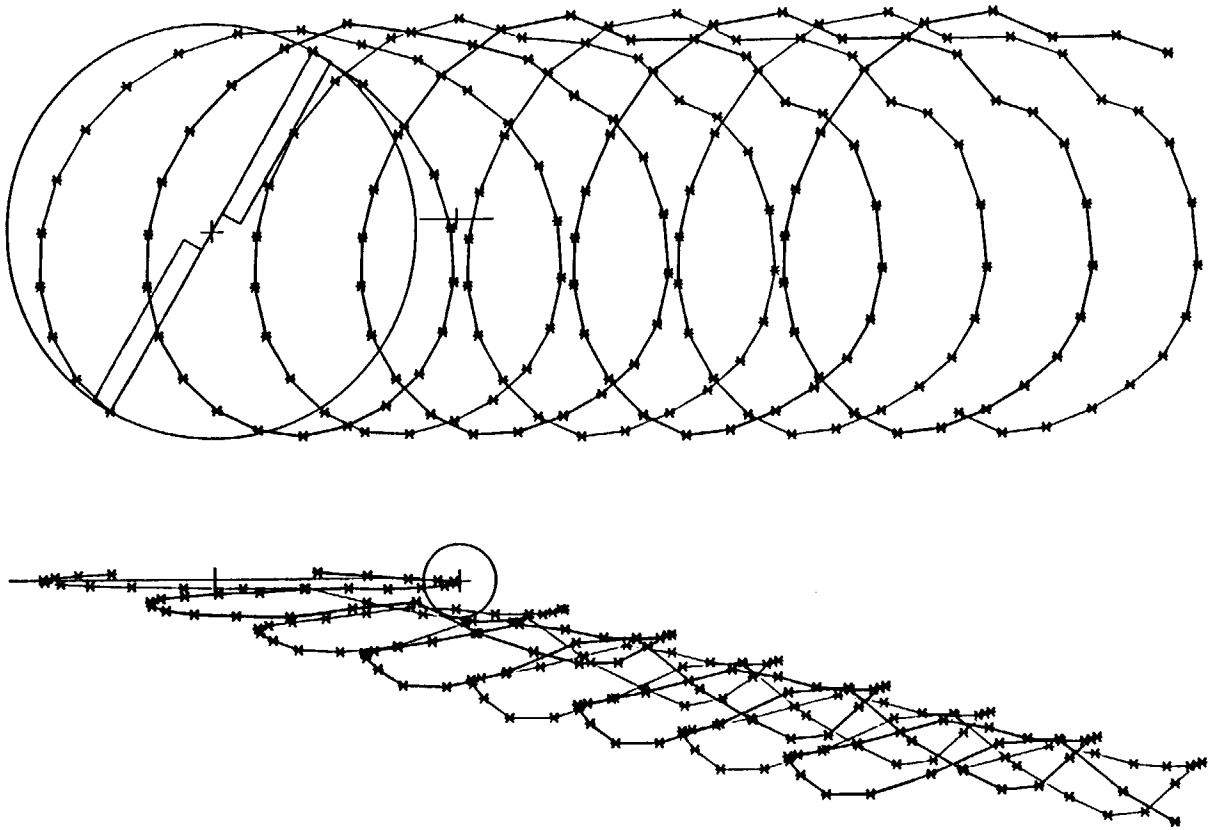

PSI = 60. DEGREES
UH-1D, 80.0 KNOTS

Figure 2 - Continued

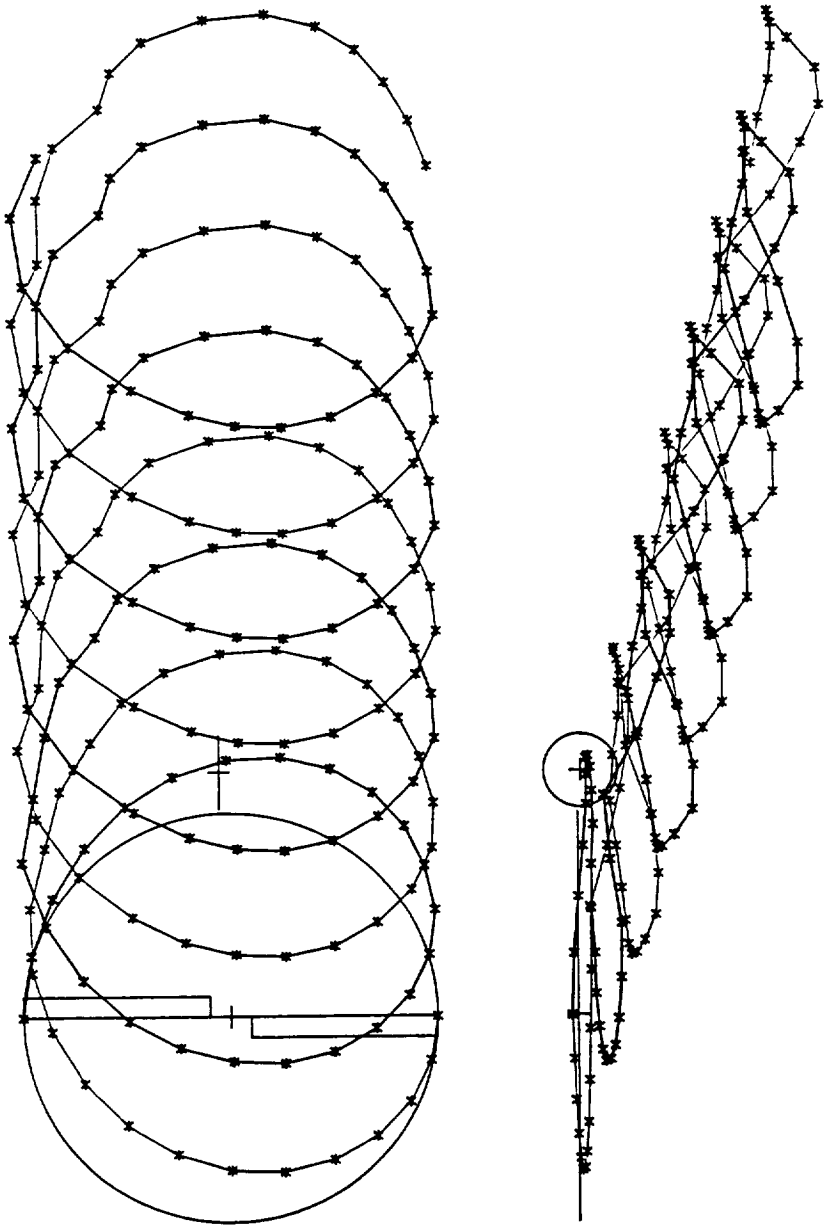

PSI = 90. DEGREES
UH-1D, 80.0 KNOTS

Figure 2 - Continued

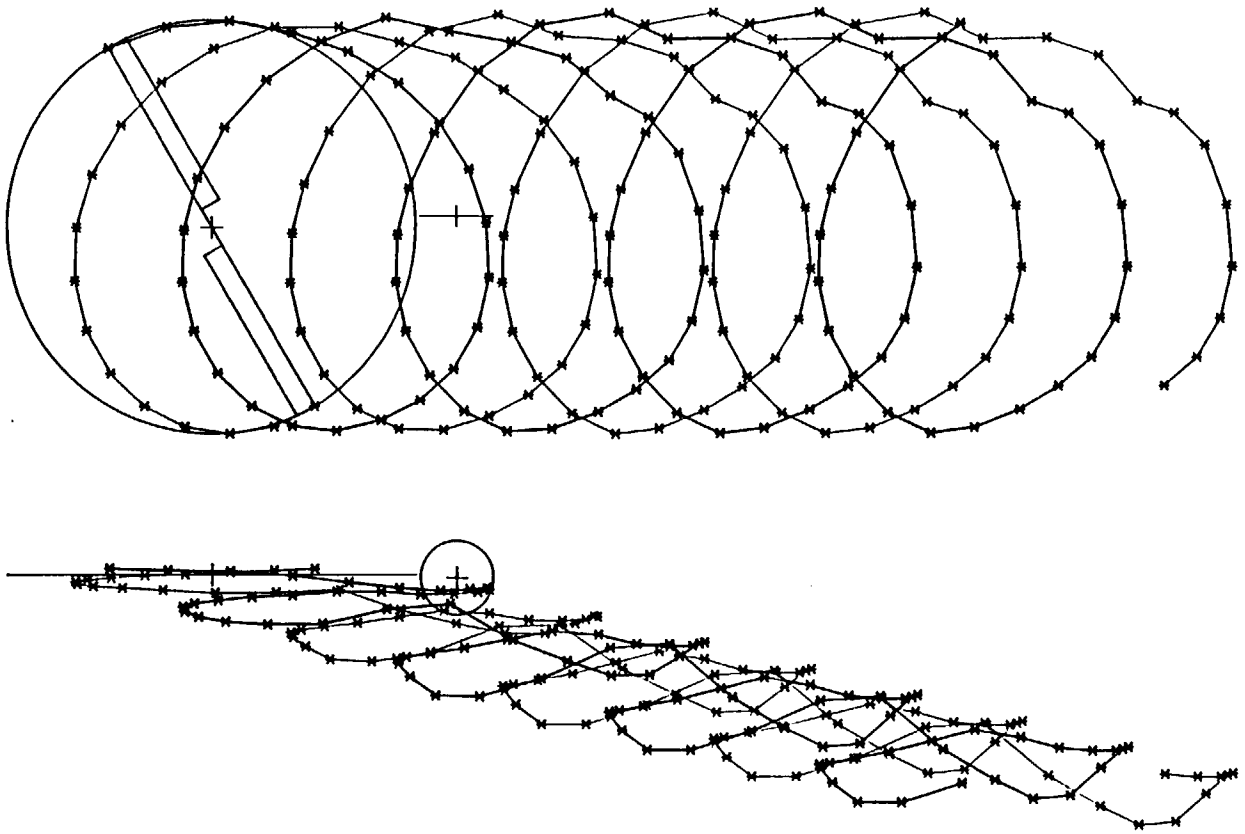

PSI = 120. DEGREES
UH-1D, 80.0 KNOTS

Figure 2 - Continued

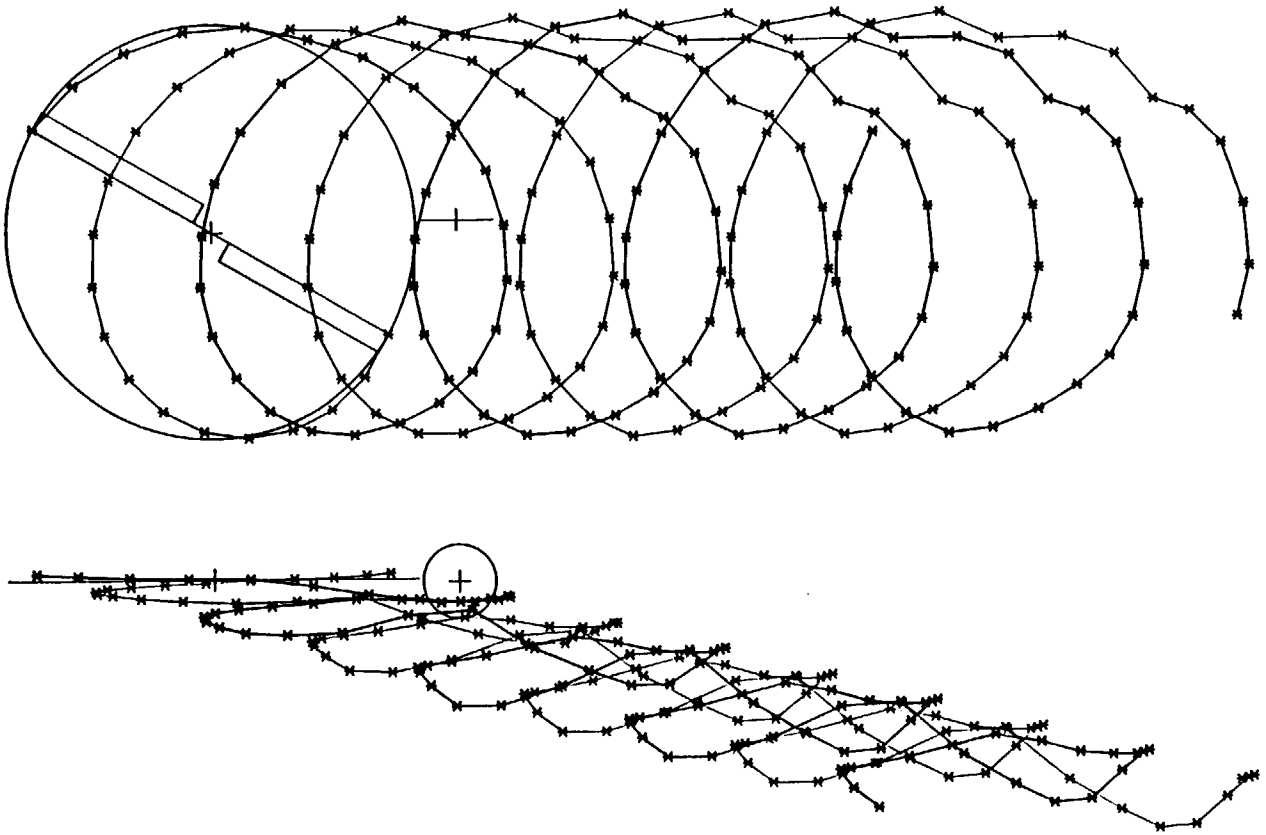

PSI = 150. DEGREES
UH-1D, 80.0 KNOTS

Figure 2 - Continued

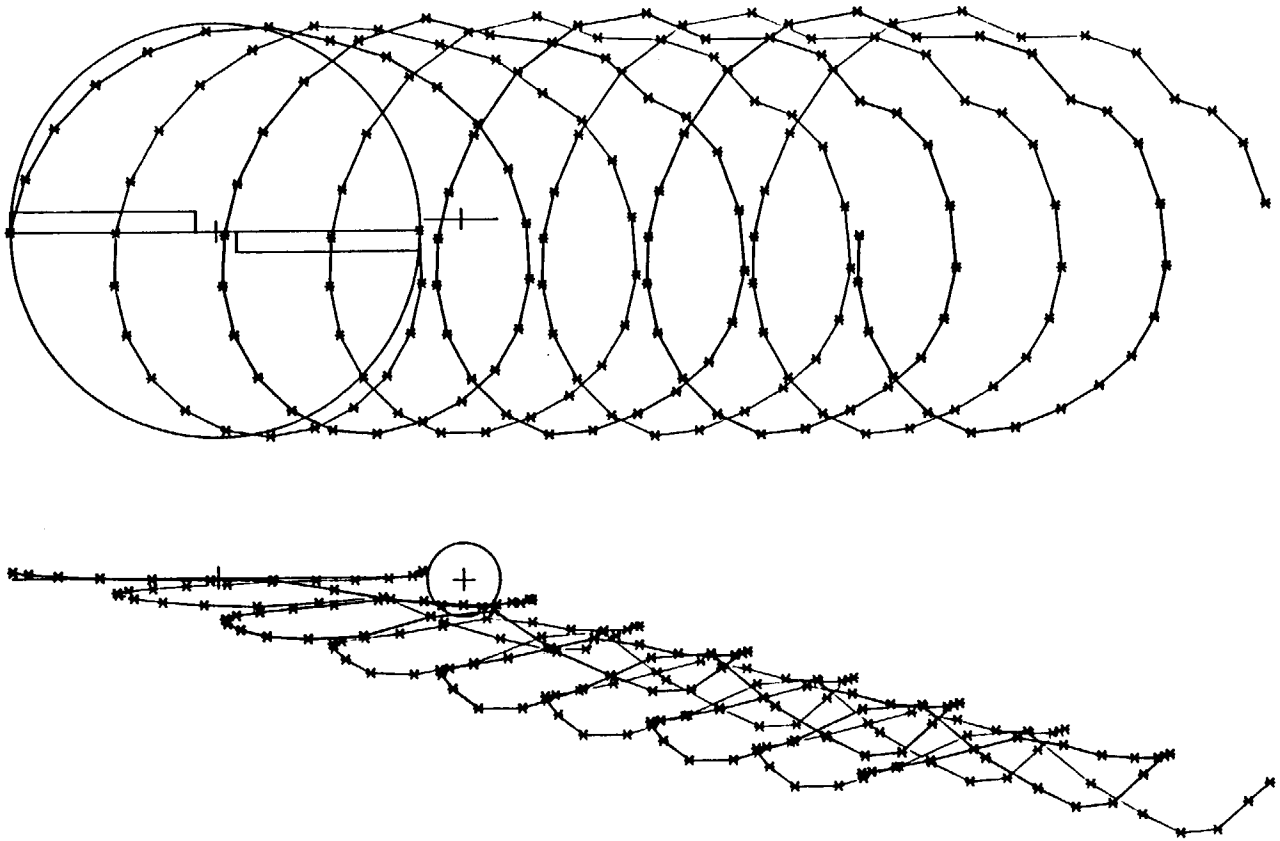

PSI = 180. DEGREES
UH-1D, 80.0 KNOTS

Figure 2 - Continued

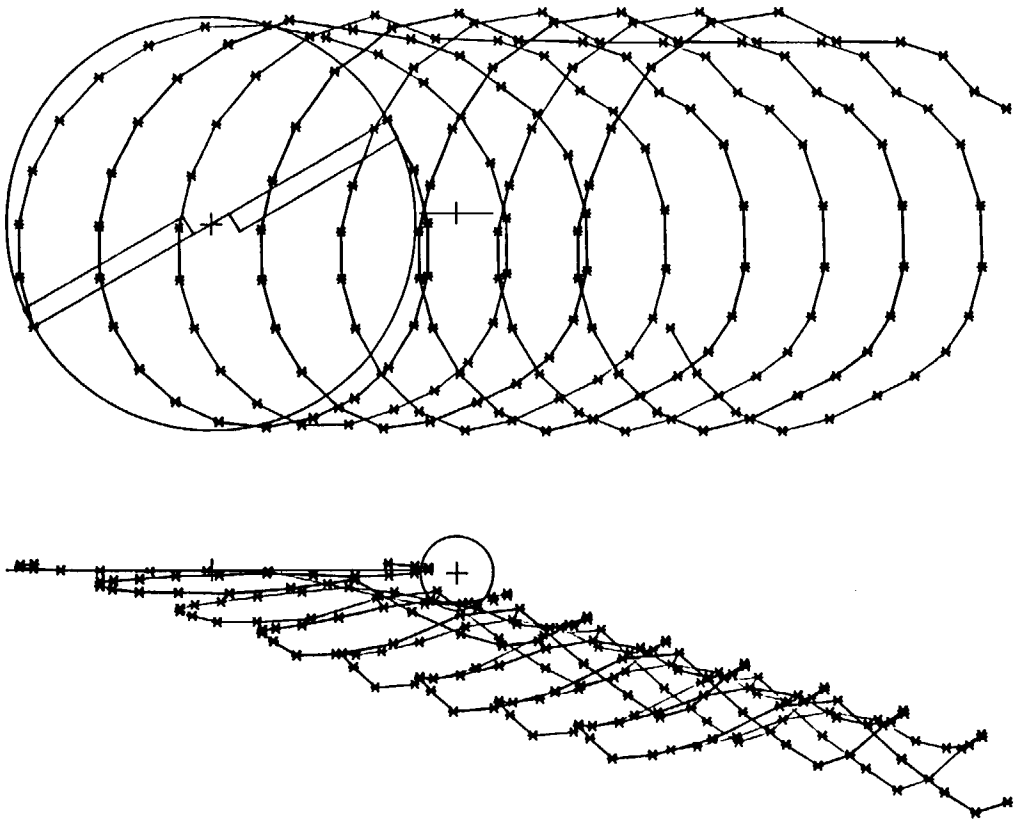

Figure 3 Free Wake Geometry Analysis Result

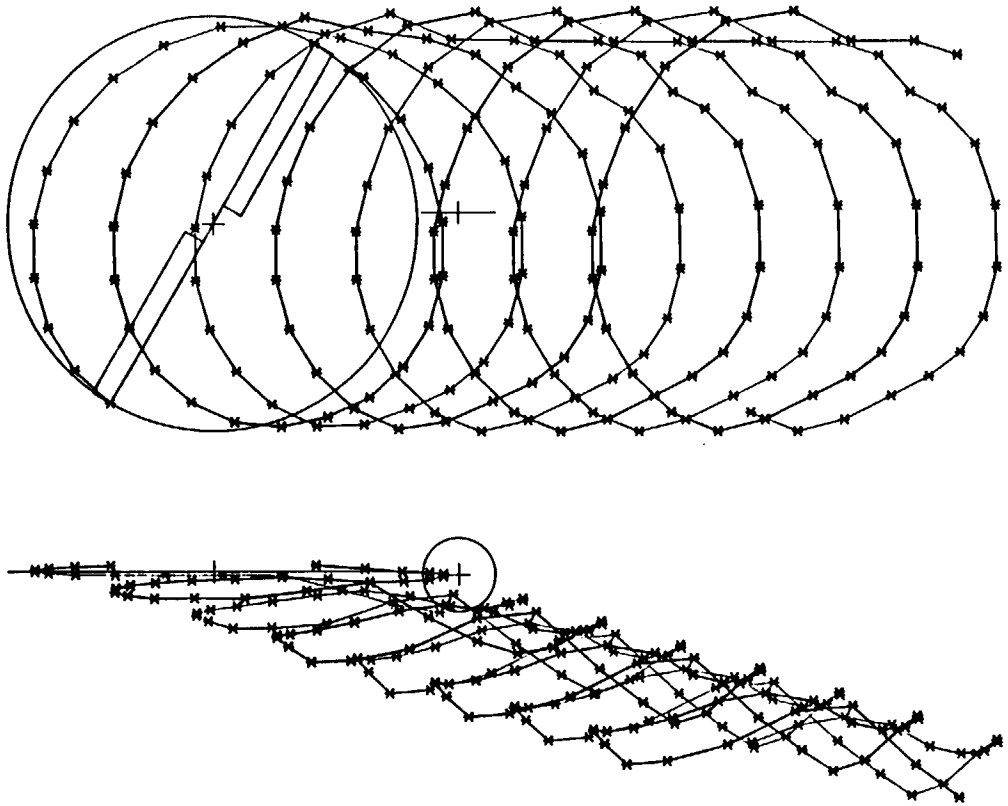

PSI = 60. DEGREES
UH-1D, 60.0 KNOTS

Figure 3 - Continued

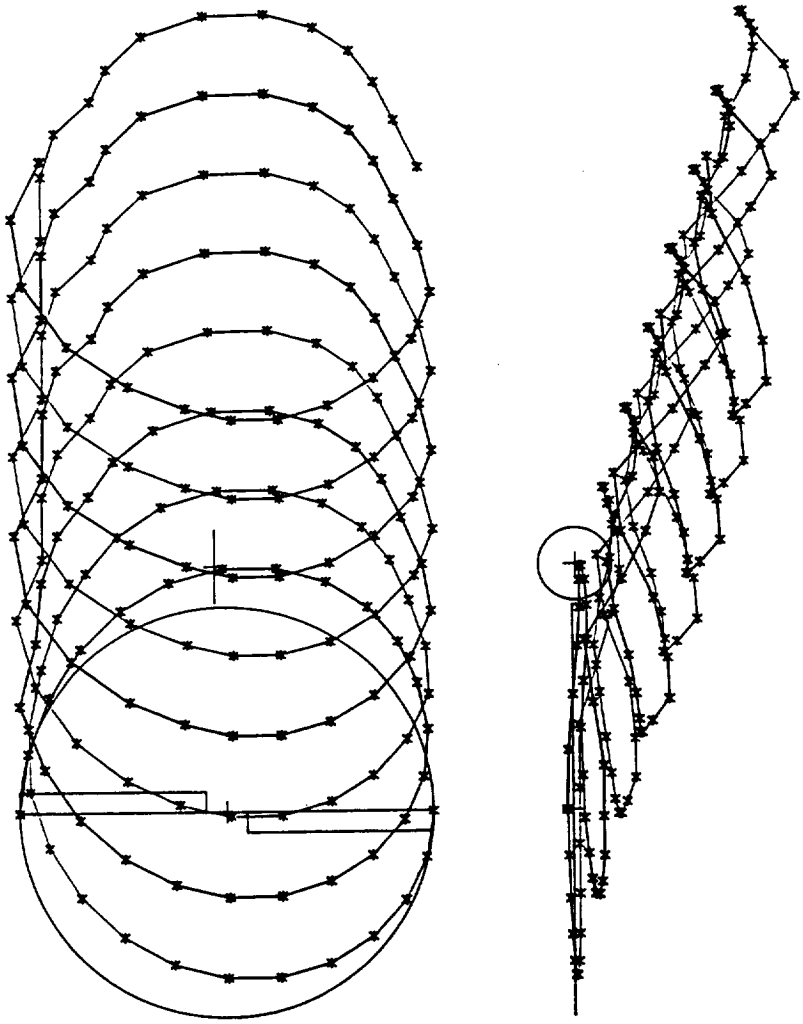

PSI = 90. DEGREES
UH-1D, 60.0 KNOTS

Figure 3 - Continued

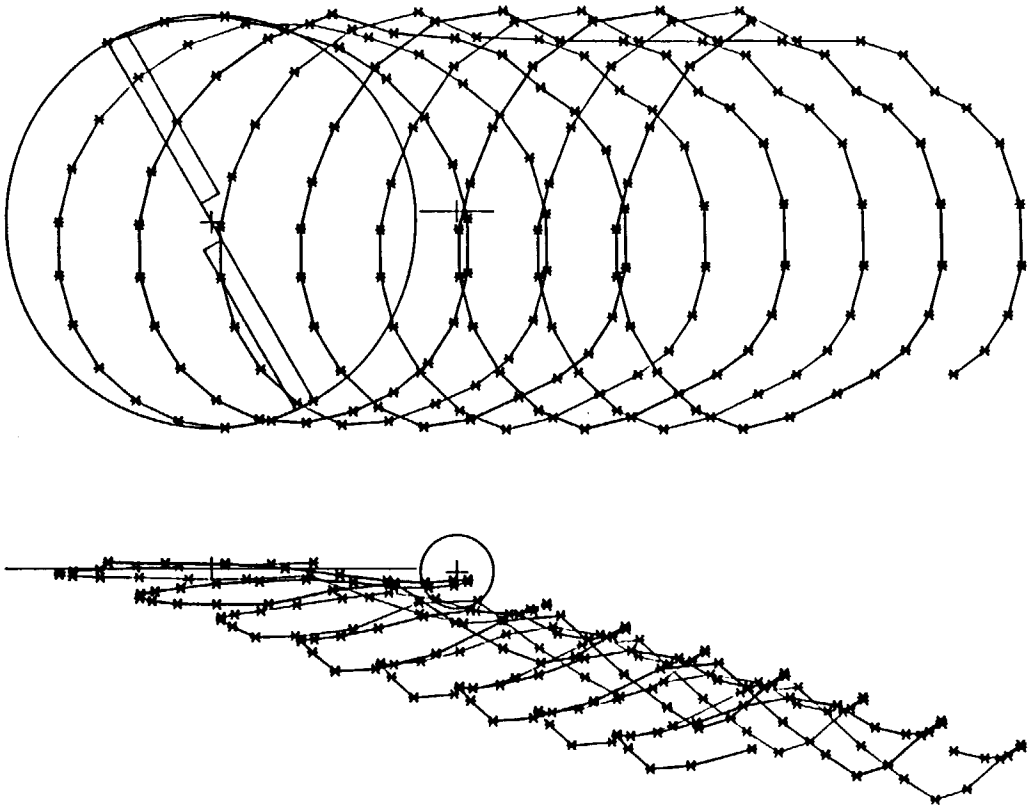

PSI = 120. DEGREES
UH-1D, 60.0 KNOTS

Figure 3 - Continued

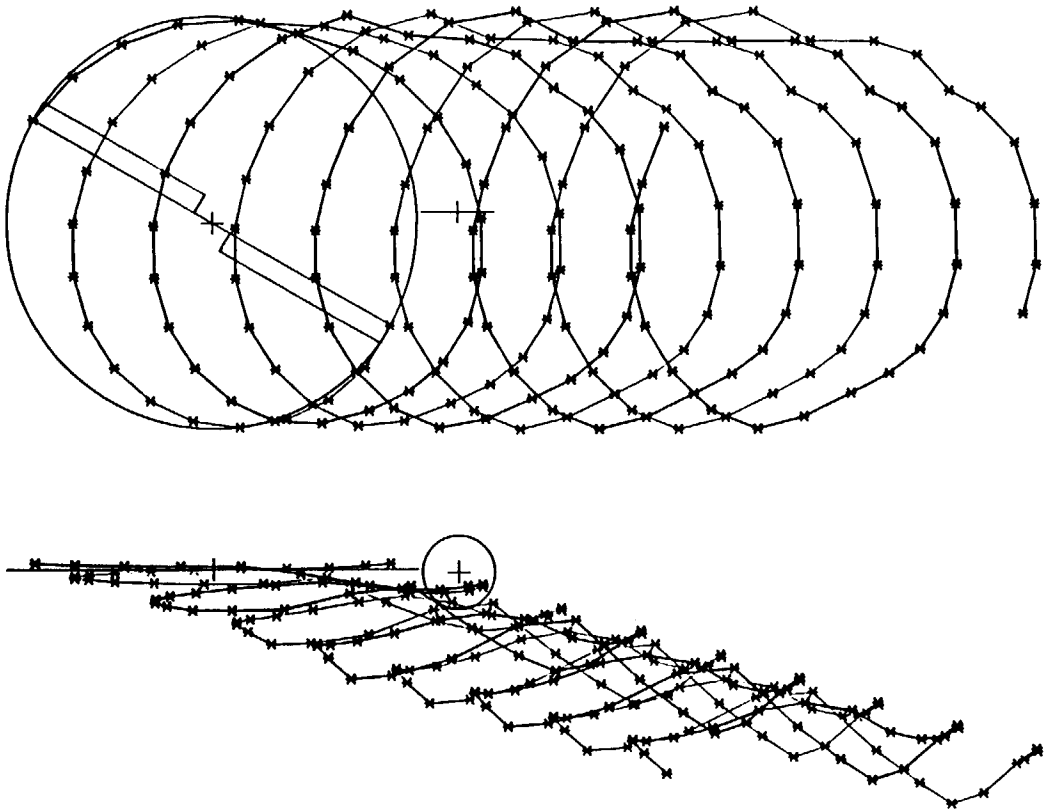

PSI = 150. DEGREES
UH-1D, 60.0 KNOTS

Figure 3 - Continued

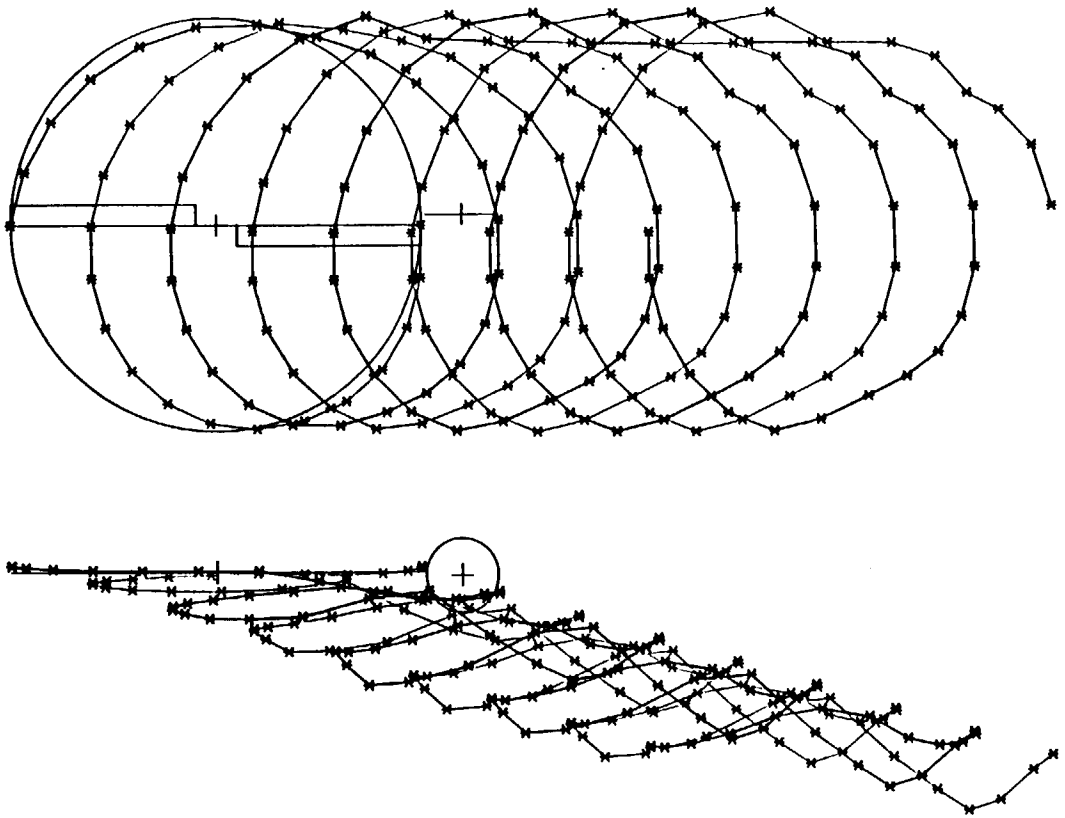

PSI = 180. DEGREES
UH-1D, 60.0 KNOTS

Figure 3 - Continued

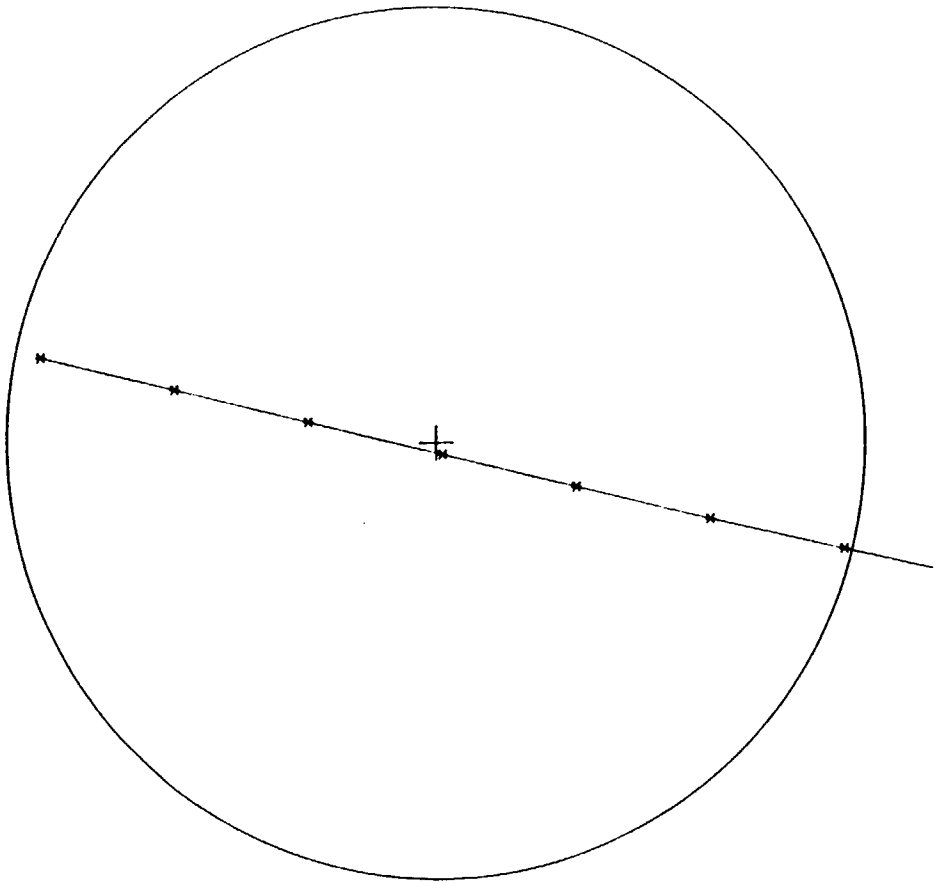

UH-1D, 100.0 KNOTS

Figure 4 Main Rotor Tip Vortex Trajectory on Tail Rotor Disk

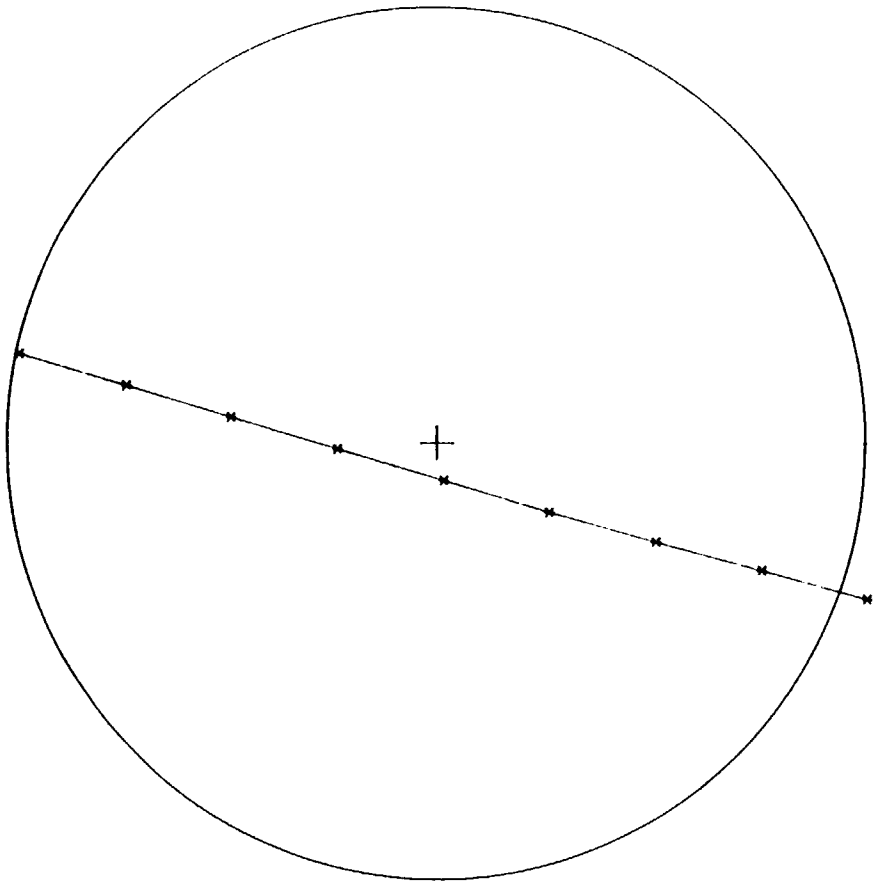

UH—1D, 80.0 KNOTS

Figure 5 Main Rotor Tip Vortex Trajectory on Tail Rotor Disk

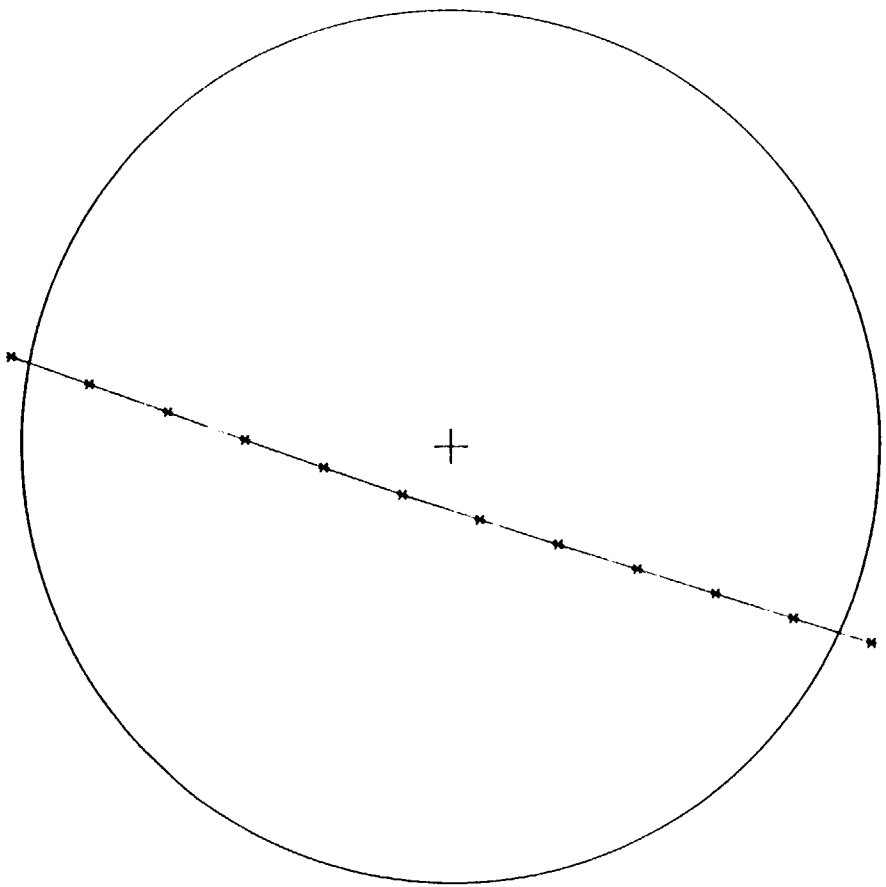

Figure 6 Main Rotor Tip Vortex Trajectory on Tail Rotor Disk

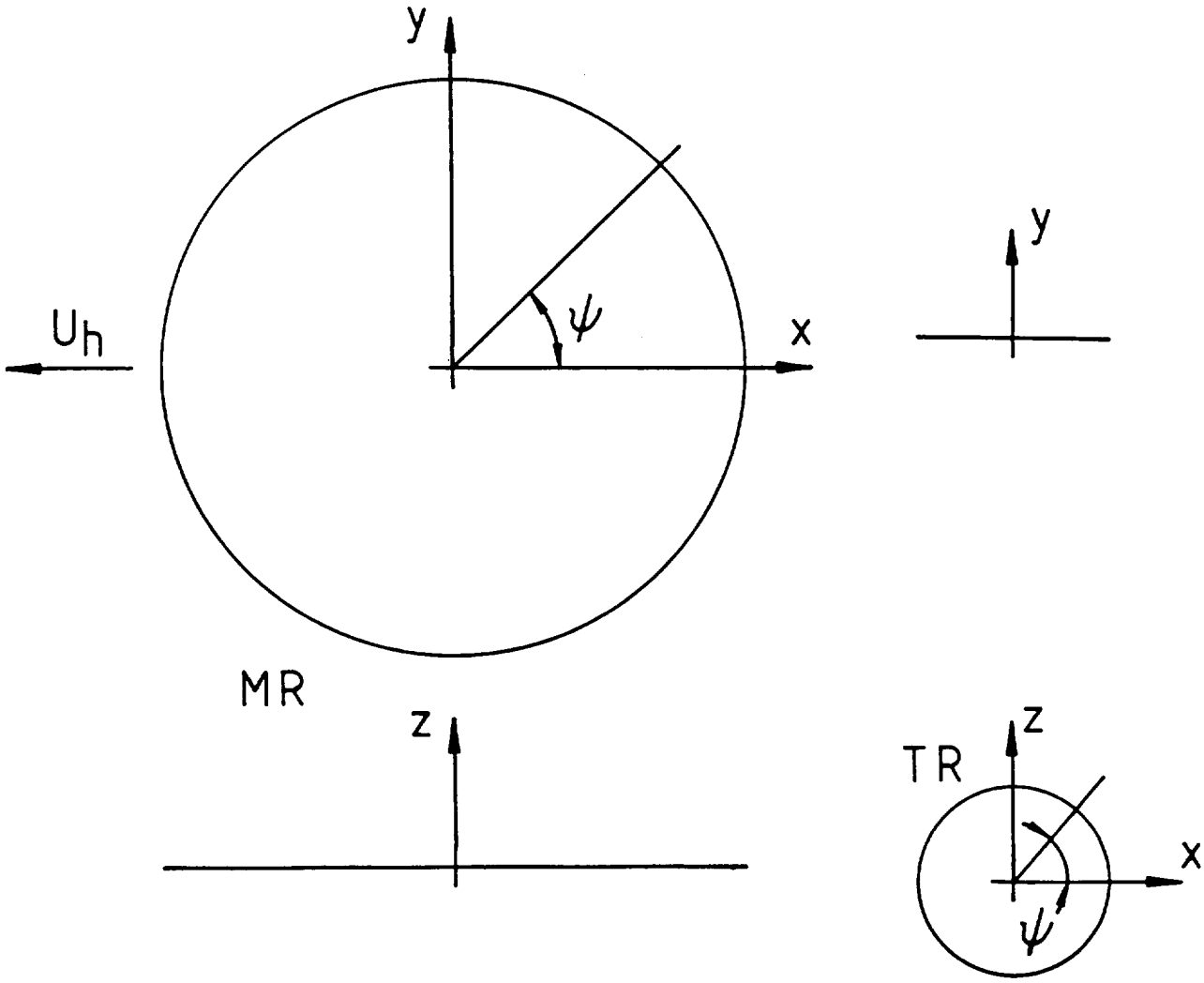

Figure 7 Definitions of Main Rotor and Tail Rotor Coordinates and Azimuthal Angles

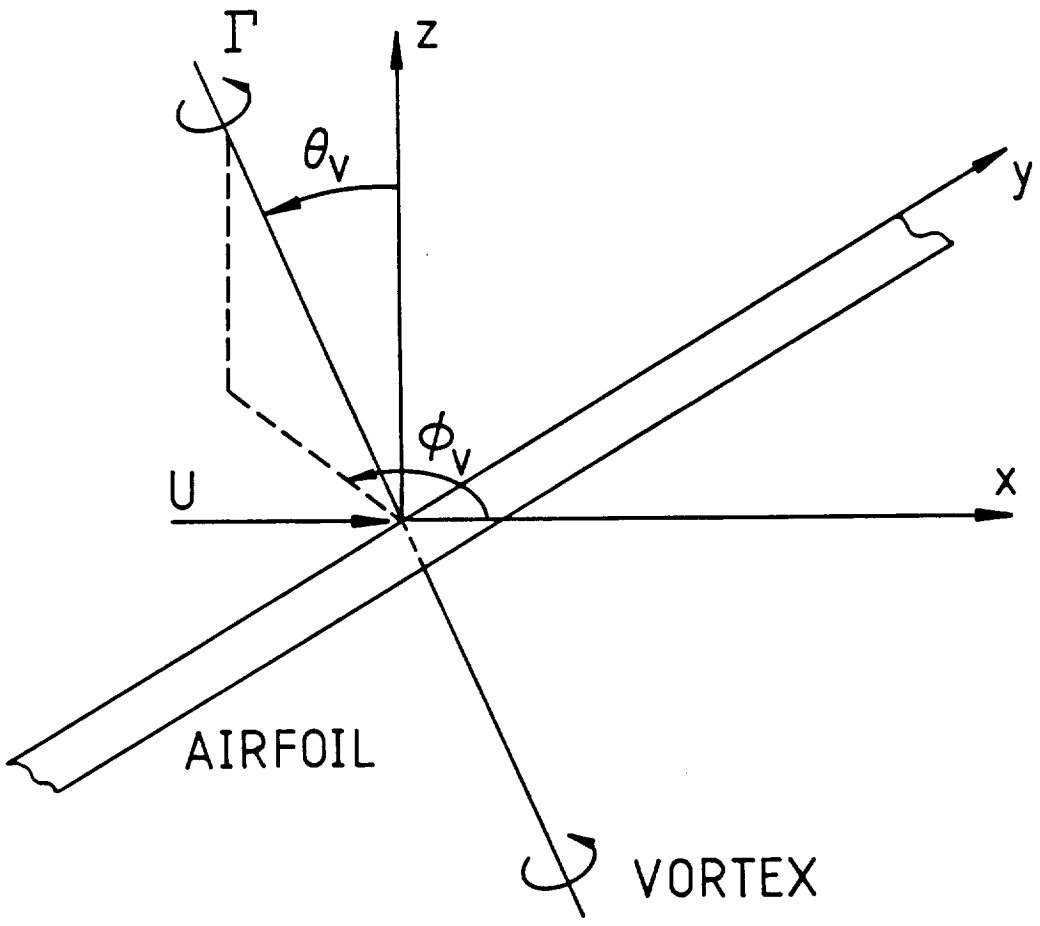

Figure 8 Definition of Tail Rotor Blade-Vortex Interaction Geometry and Vortex Orientation

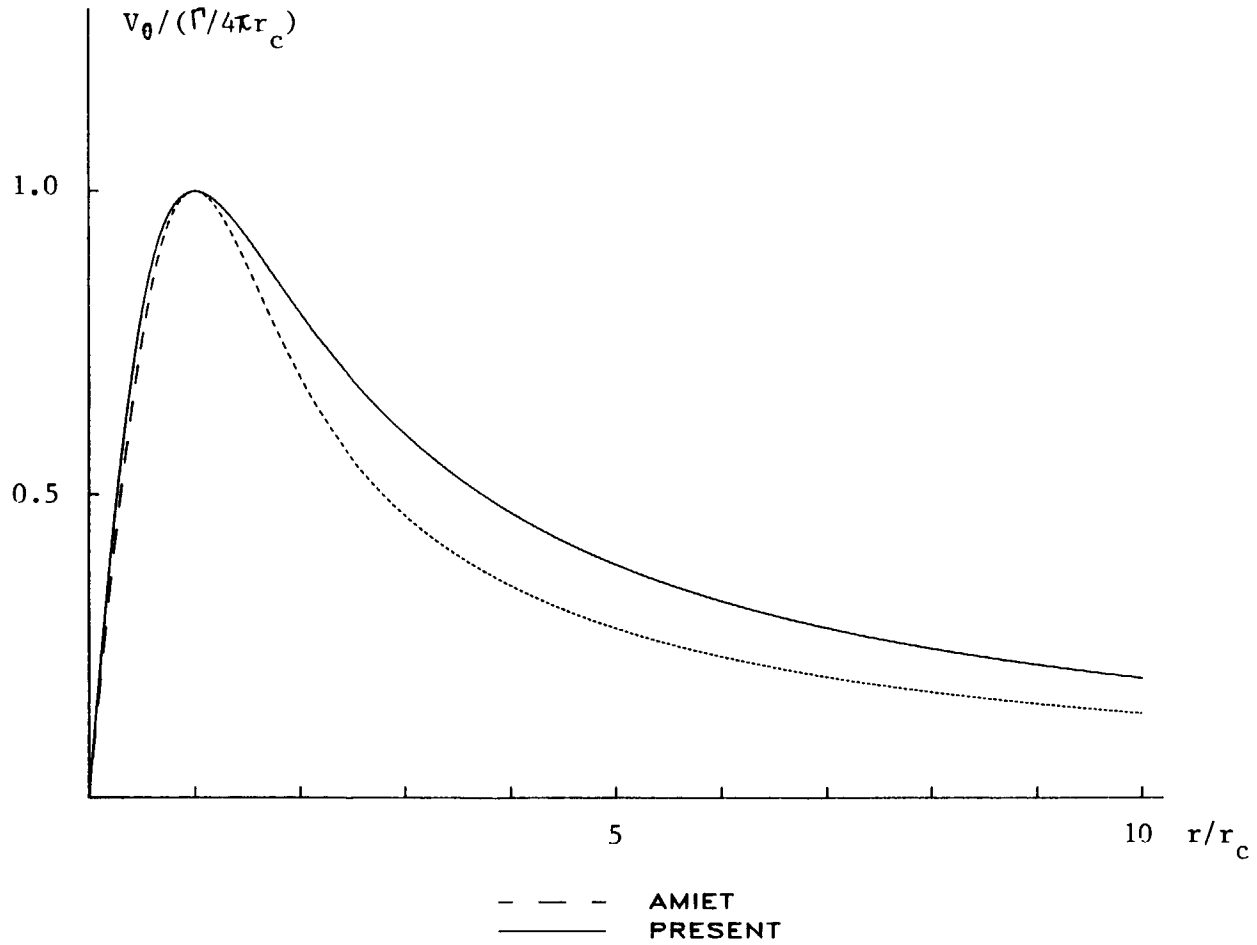

Figure 9 COMPARISON OF VORTEX MODELS

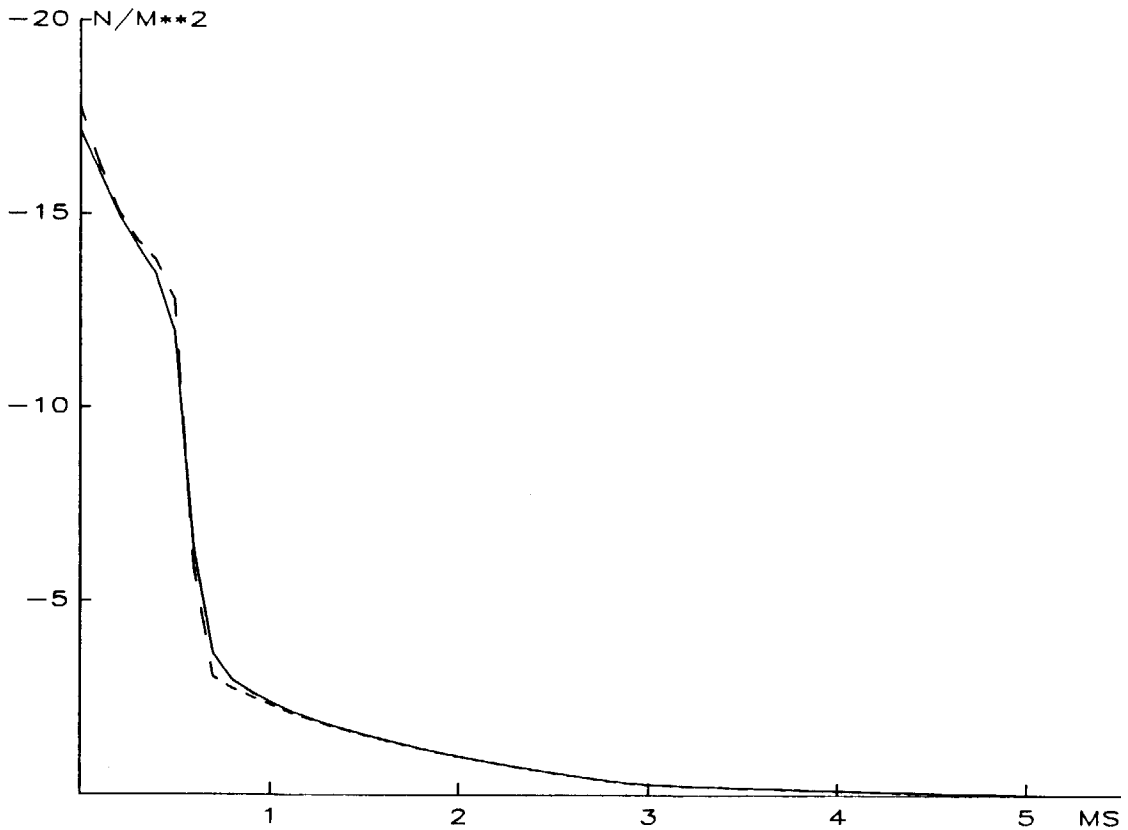

Figure 10 COMPARISON OF BVI NOISE USING DIFFERENT VORTEX MODELS

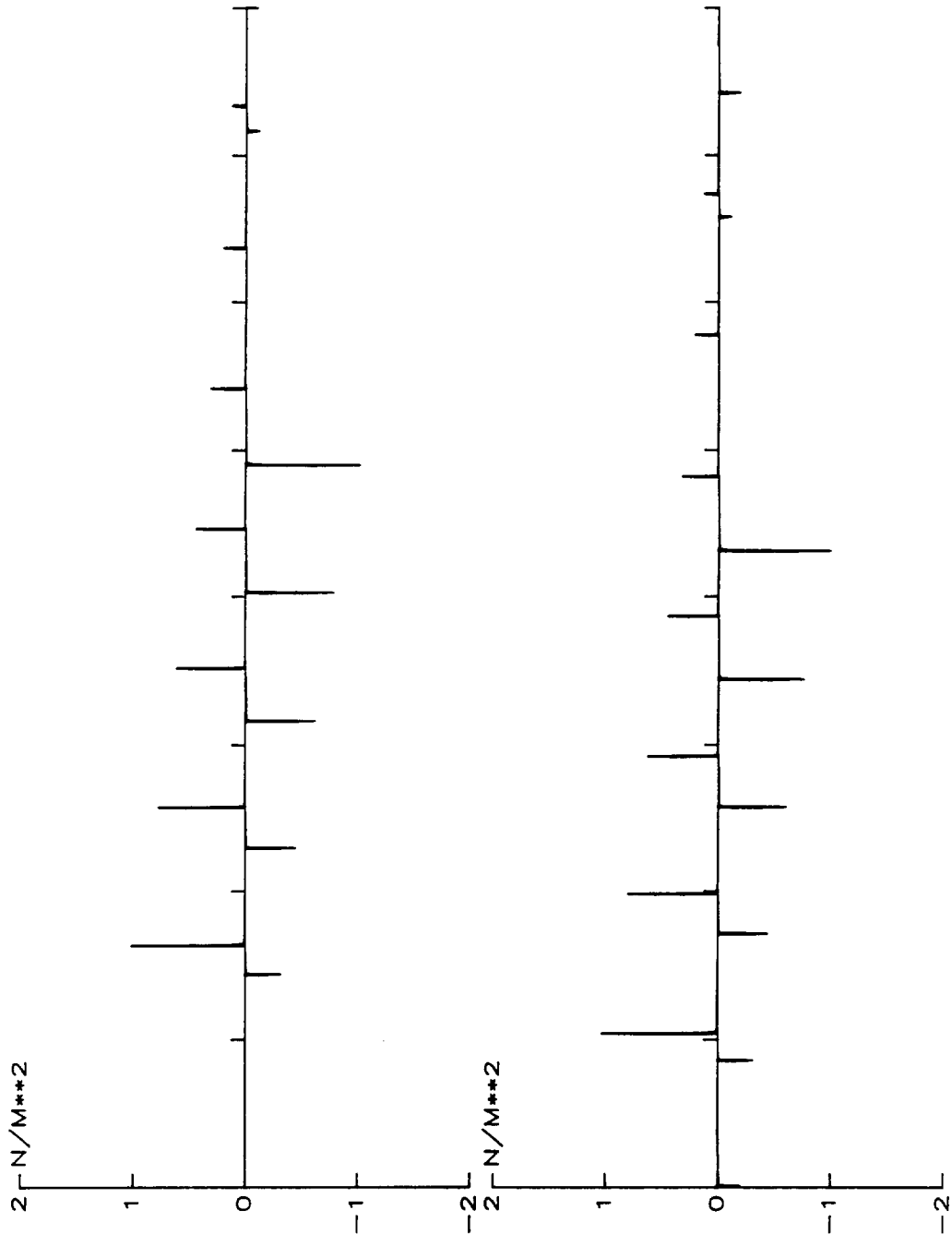

Figure 11 Sound Pressure-Time History for Tail Rotor Blade-Vortex Interaction

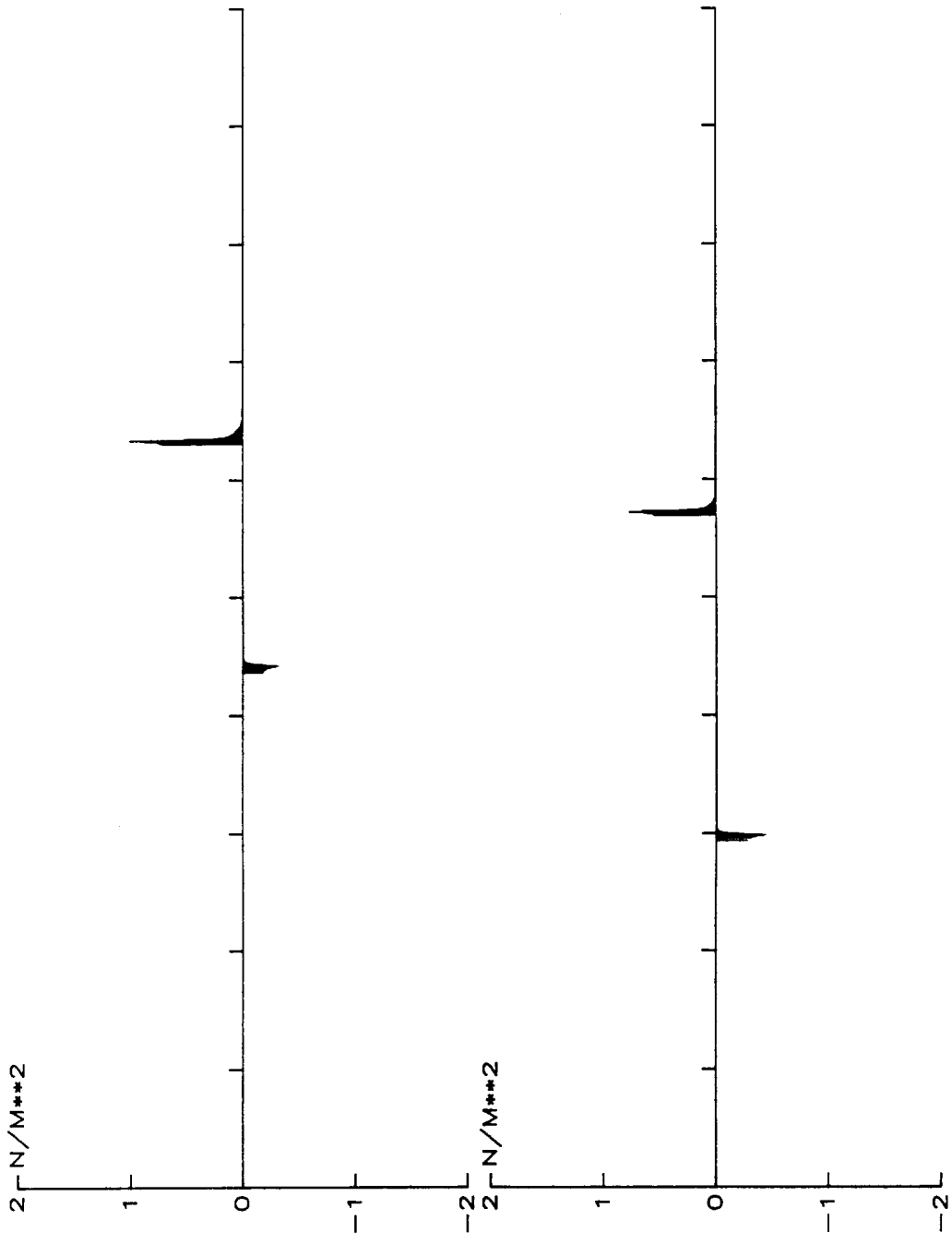

Figure 12 Sound Pressure-Time History for Tail Rotor Blade-Vortex Interaction

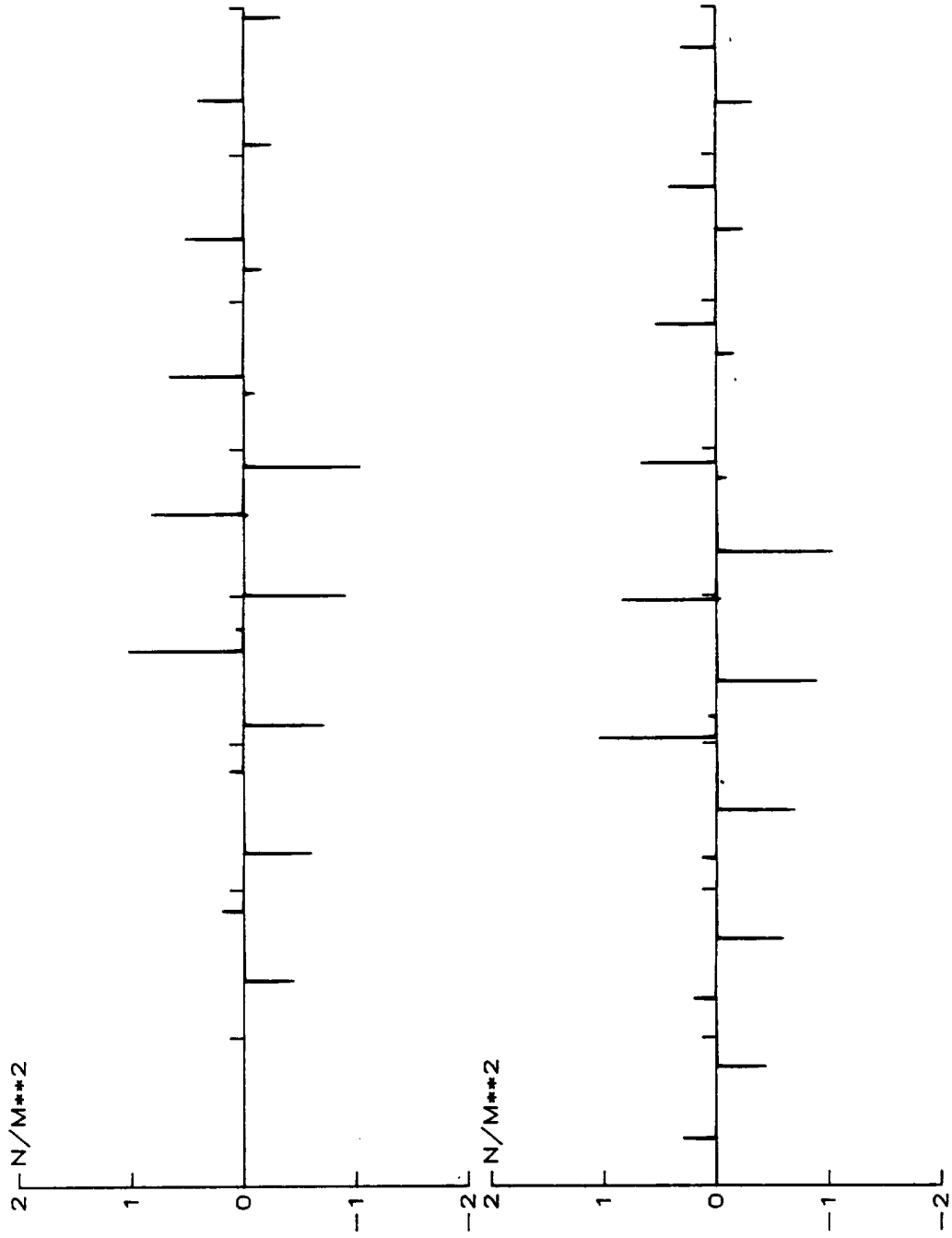

Figure 13 Sound Pressure-Time History for Tail Rotor-Blade-Vortex Interaction

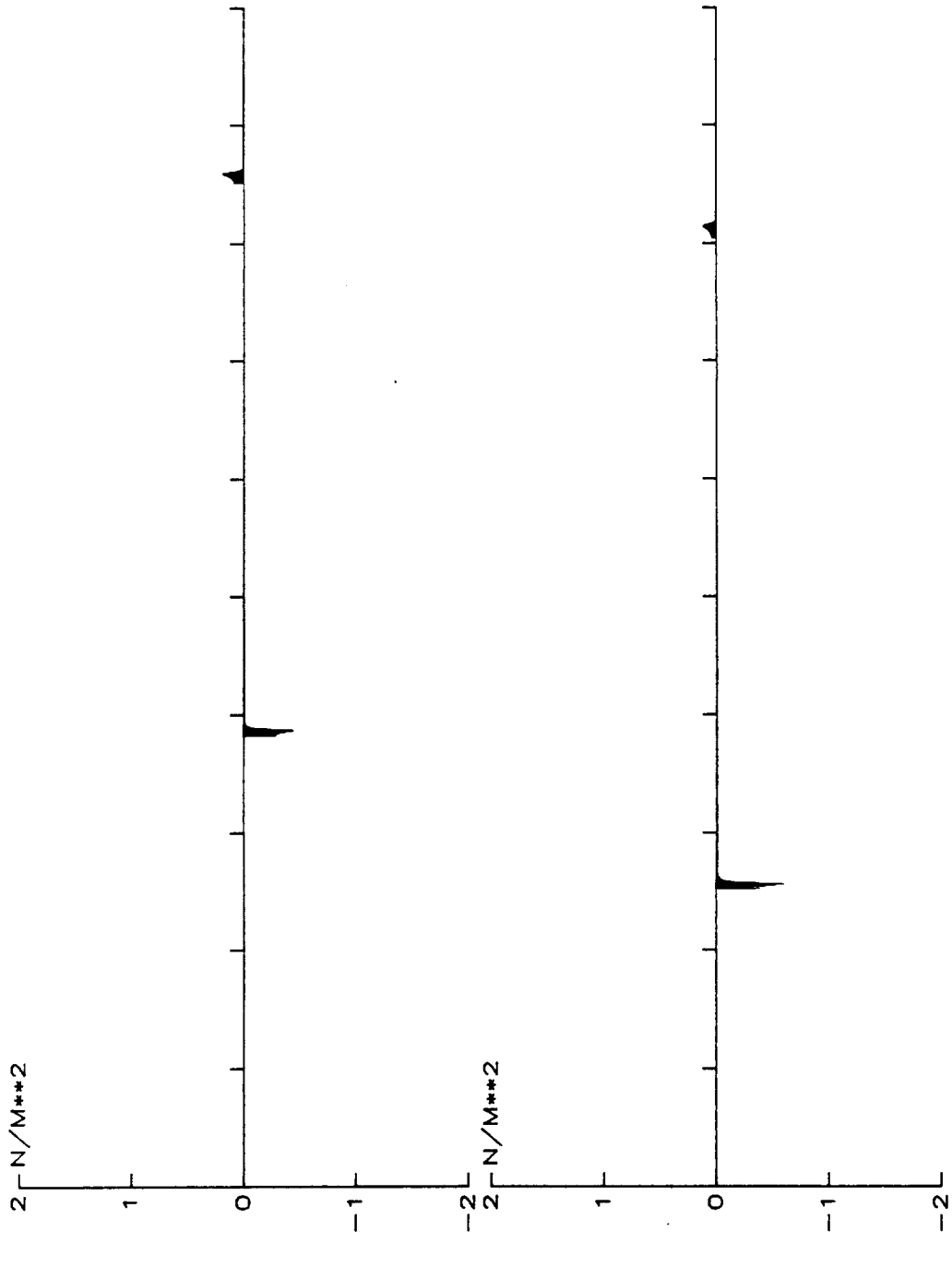

Figure 14 Sound Pressure-Time History for Tail Rotor Blade-Vortex Interaction

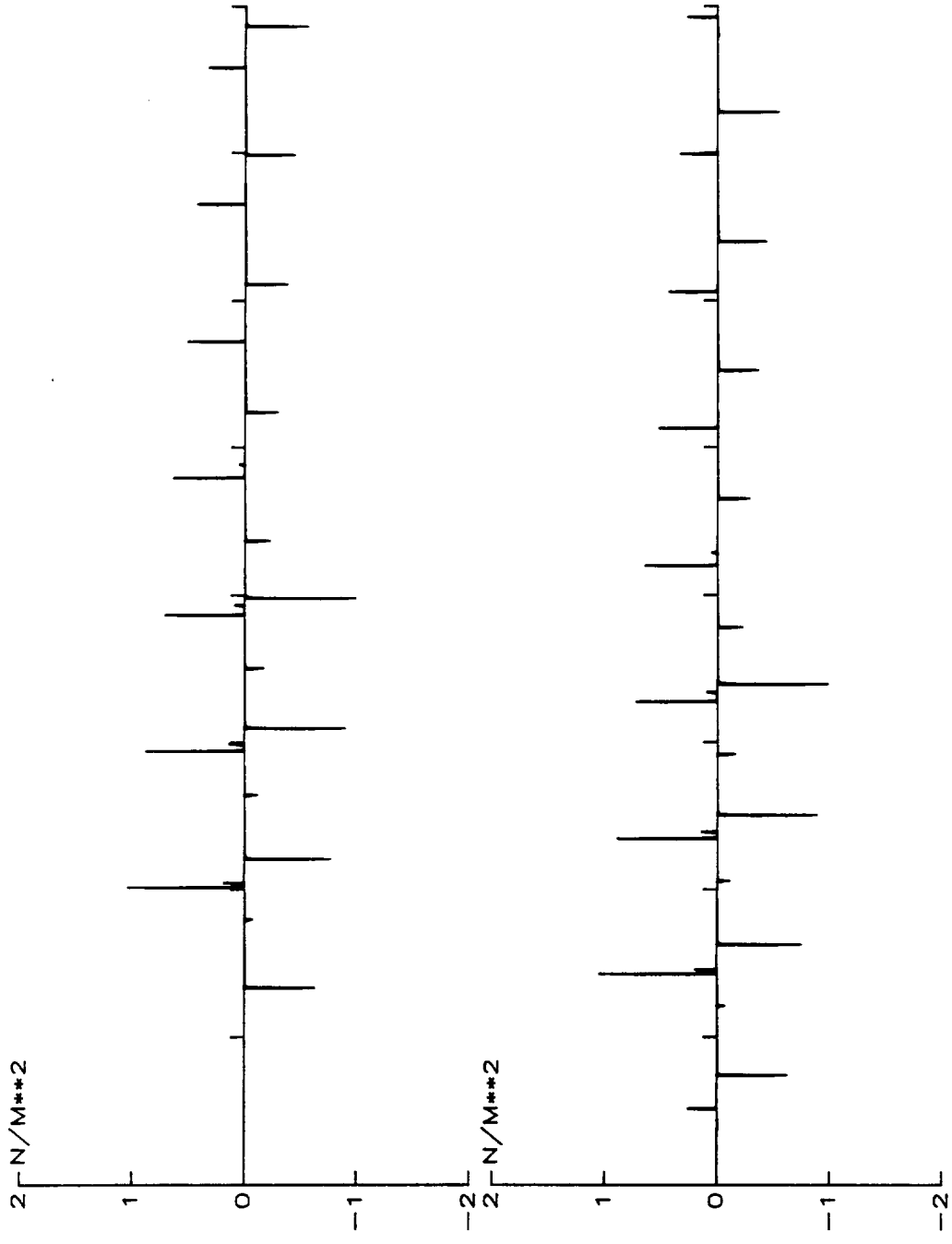

Figure 15 Sound Pressure-Time History for Tail Rotor Blade-Vortex Interaction

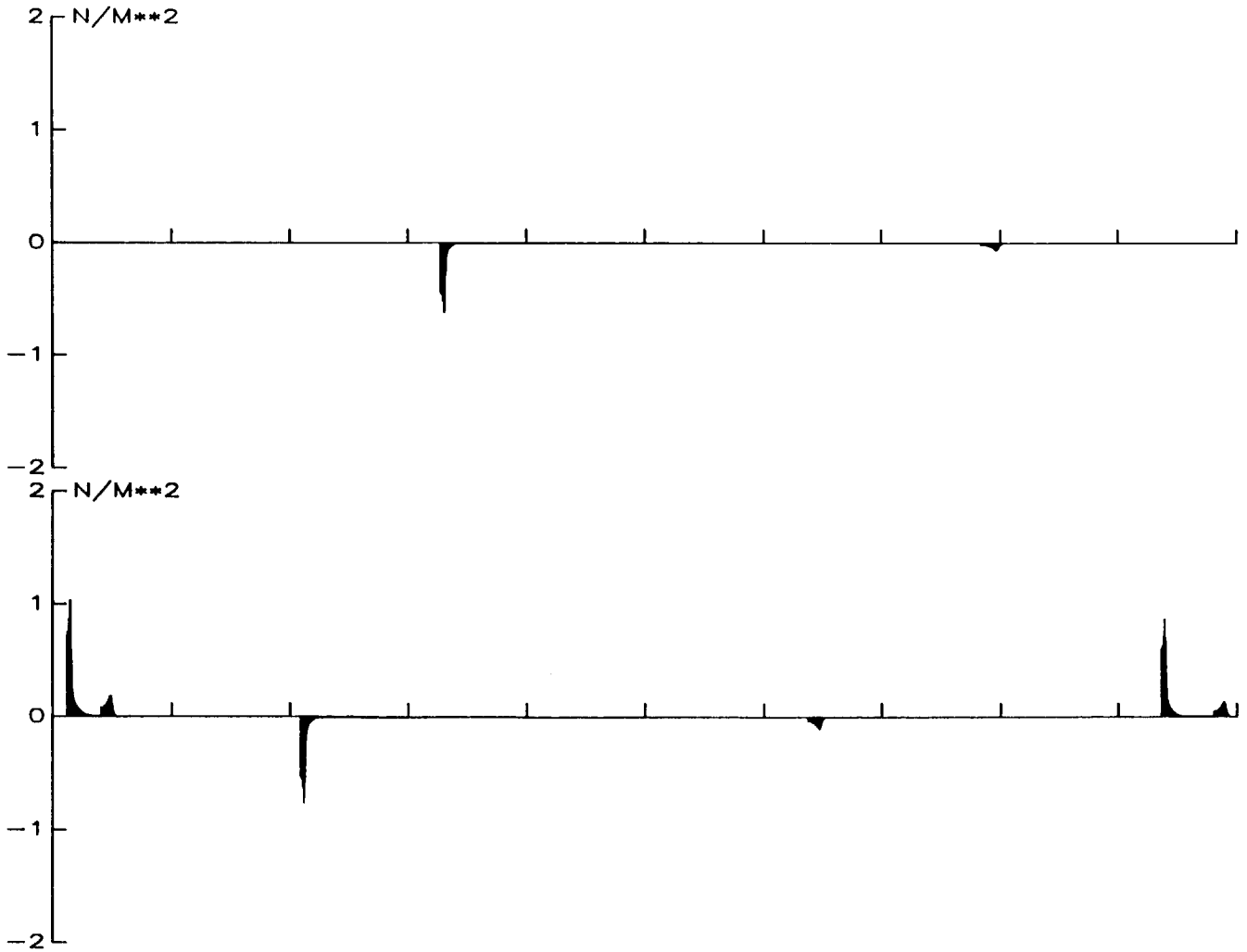

Figure 16 Sound Pressure-Time History for Tail Rotor Blade-Vortex Interaction

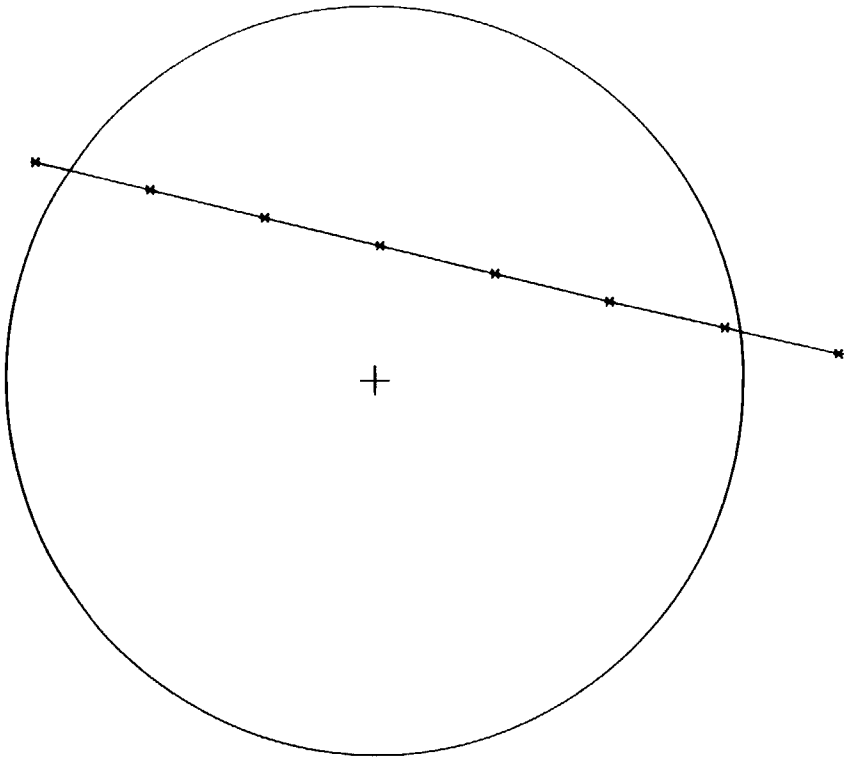

UH-1D, 100.0 KNOTS
LOWERED TAIL ROTOR

Figure 17 Main Rotor Tip Vortex Trajectory on Tail Rotor Disk

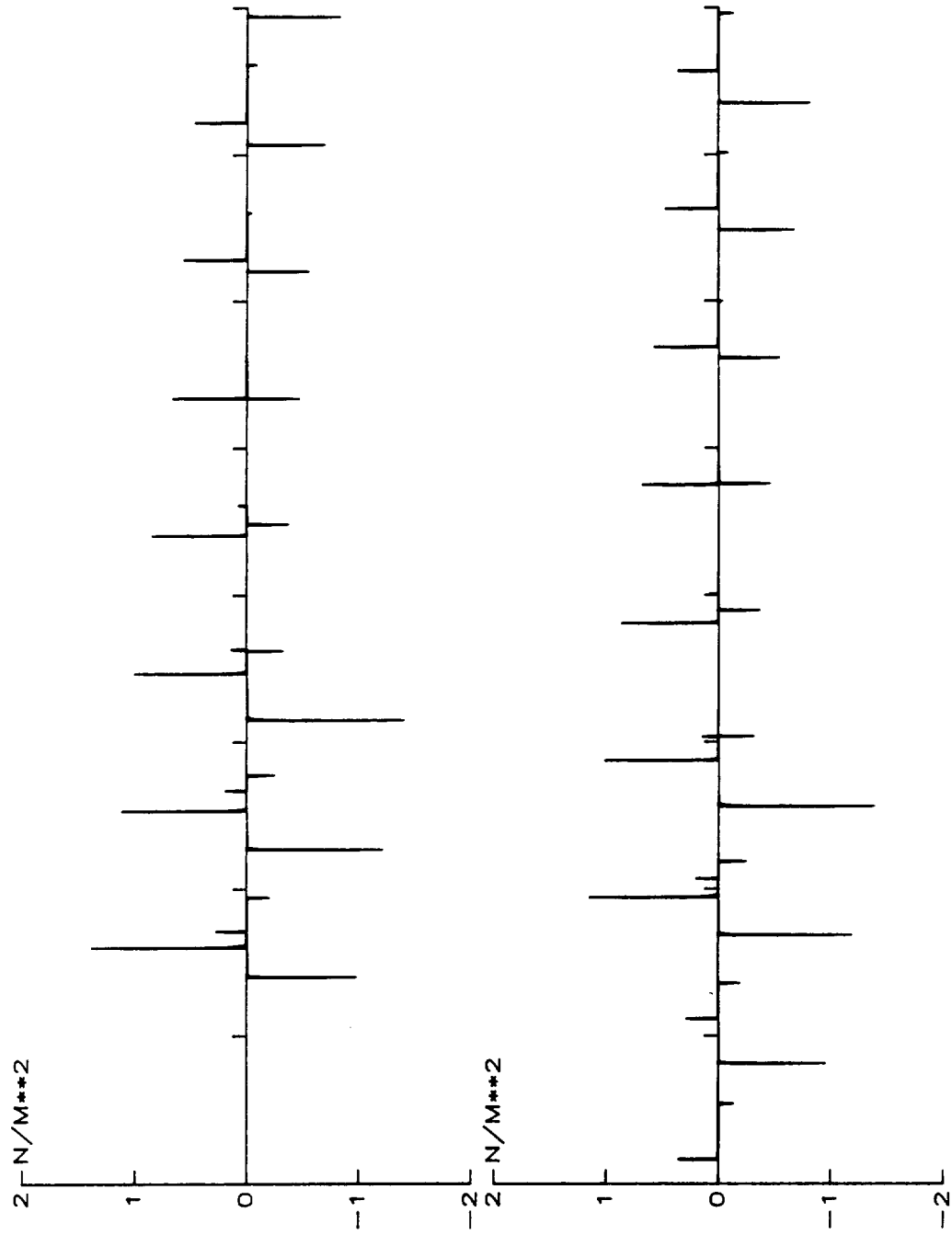

Figure 18 Sound Pressure-Time History for Tail Rotor Blade-Vortex Interaction (Tail Rotor Lowered)

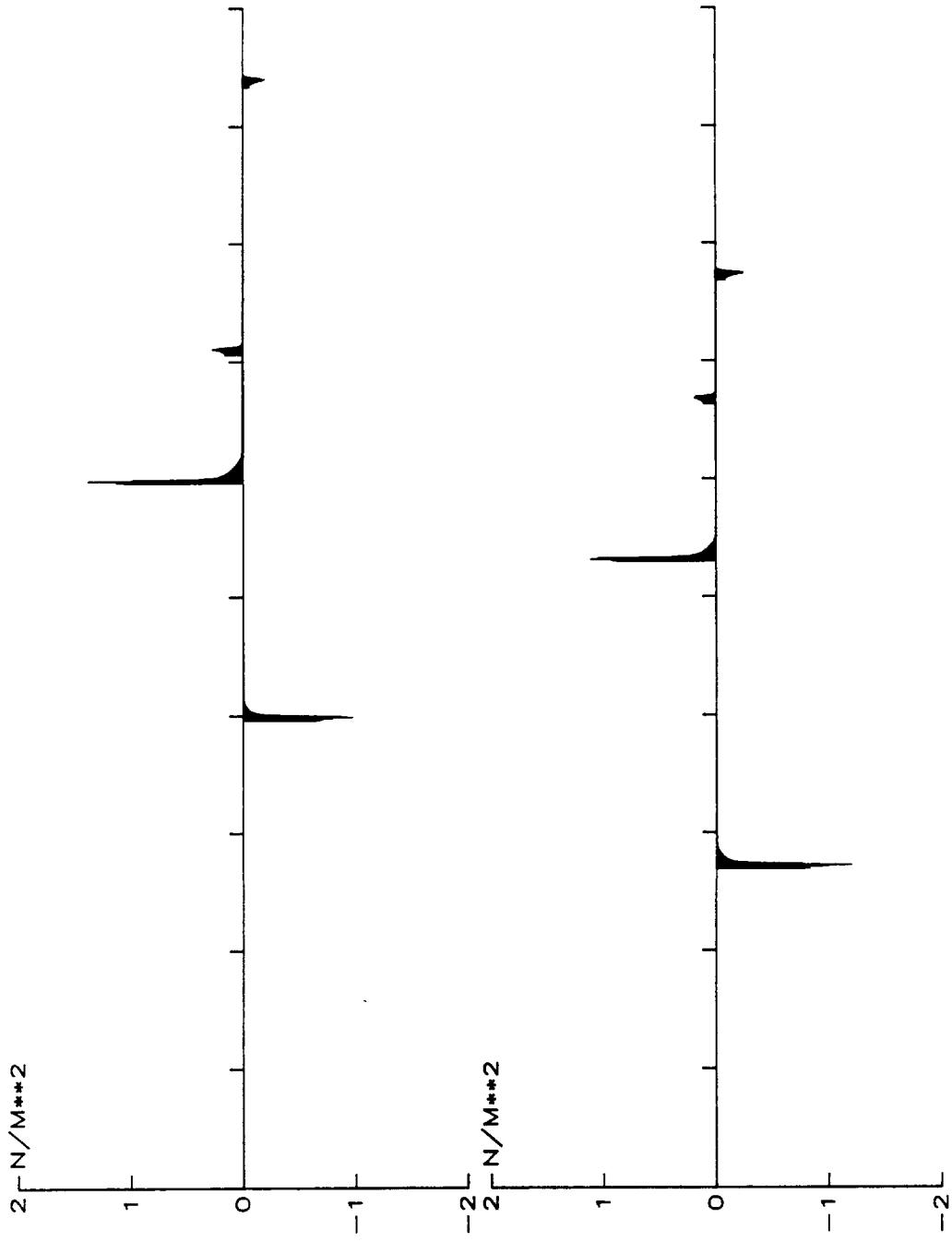

Figure 19 Sound Pressure-Time History for Tail Rotor Blade-Vortex Interaction (Tail Rotor Lowered)

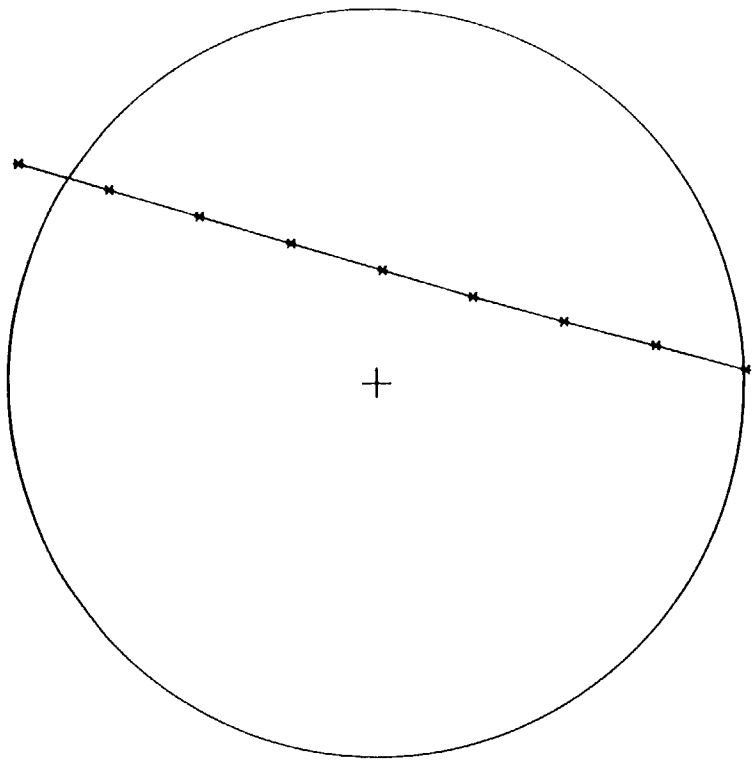

UH—1D, 80.0 KNOTS
LOWERED TAIL ROTOR

Fifure 20 Main Rotor Tip Vortex Trajectory on Tail Rotor Disk

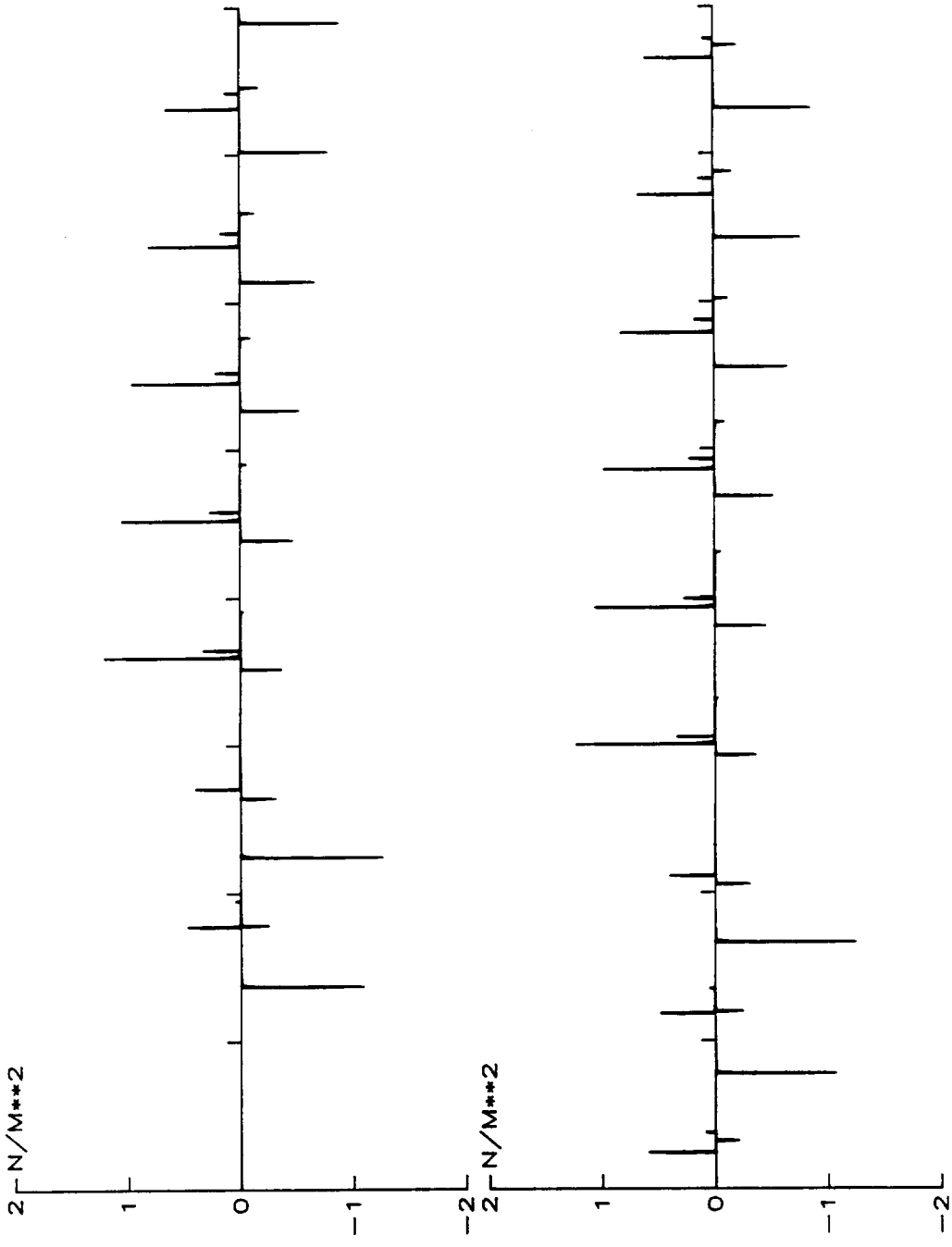

Figure 21 Sound Pressure-Time History for Tail Rotor Blade-Vortex Interaction (Tail Rotor Lowered)

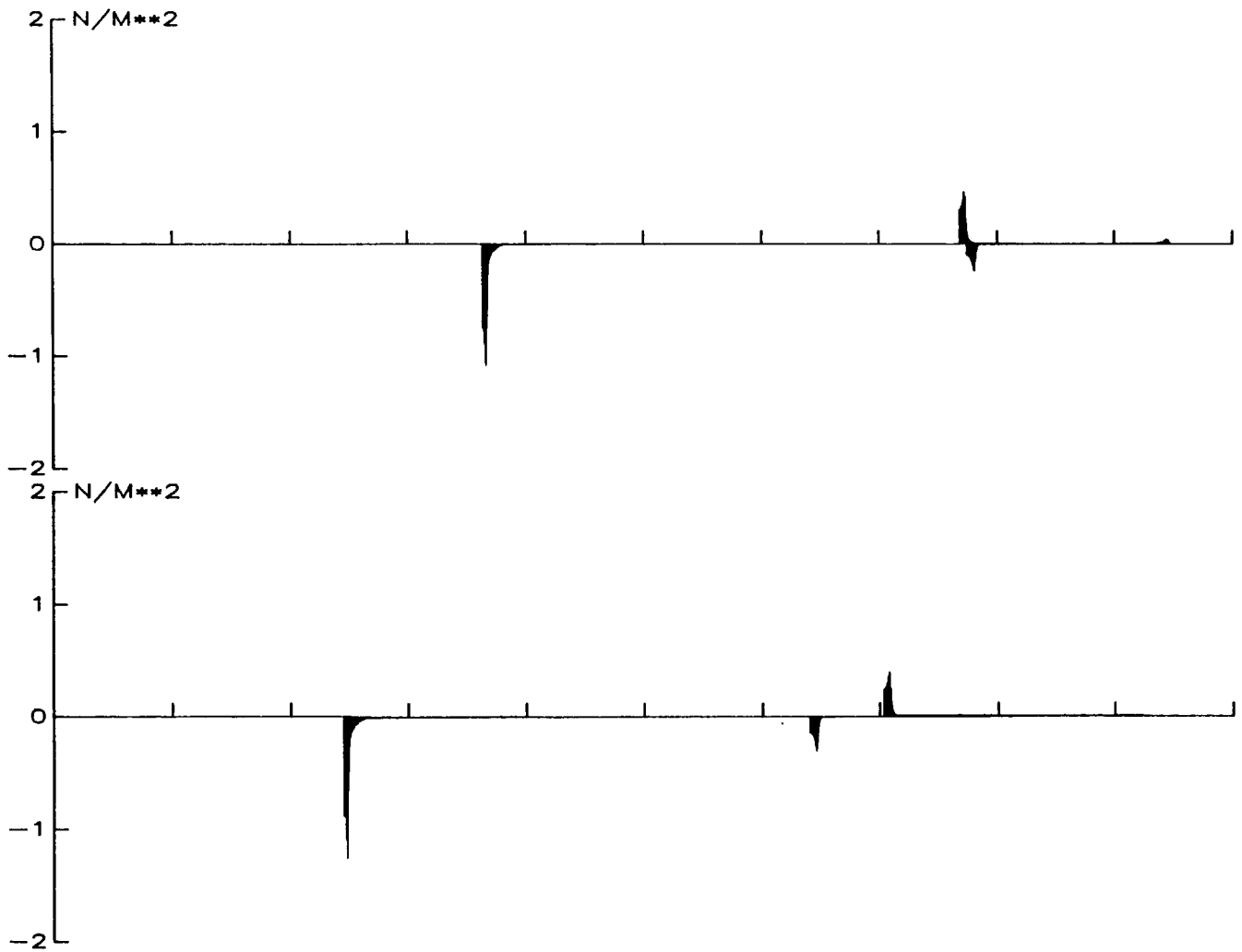

Figure 22 Sound Pressure-Time History for Tail Rotor Blade-Vortex Interaction (Tail Rotor Lowered)

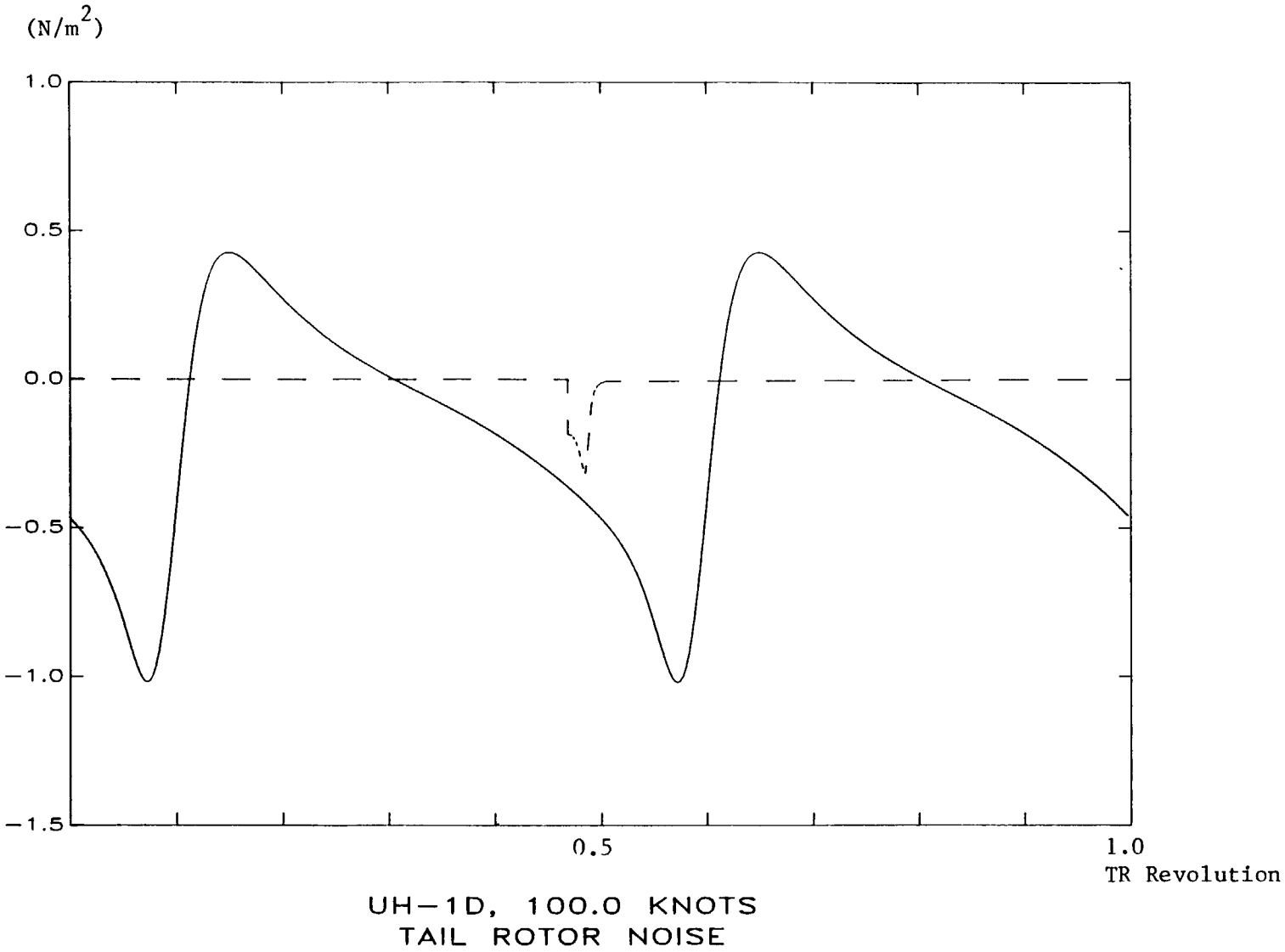

Figure 23 Comparison of Tail Rotor Blade-Vortex Interaction Noise with Thickness/ Loading Noise

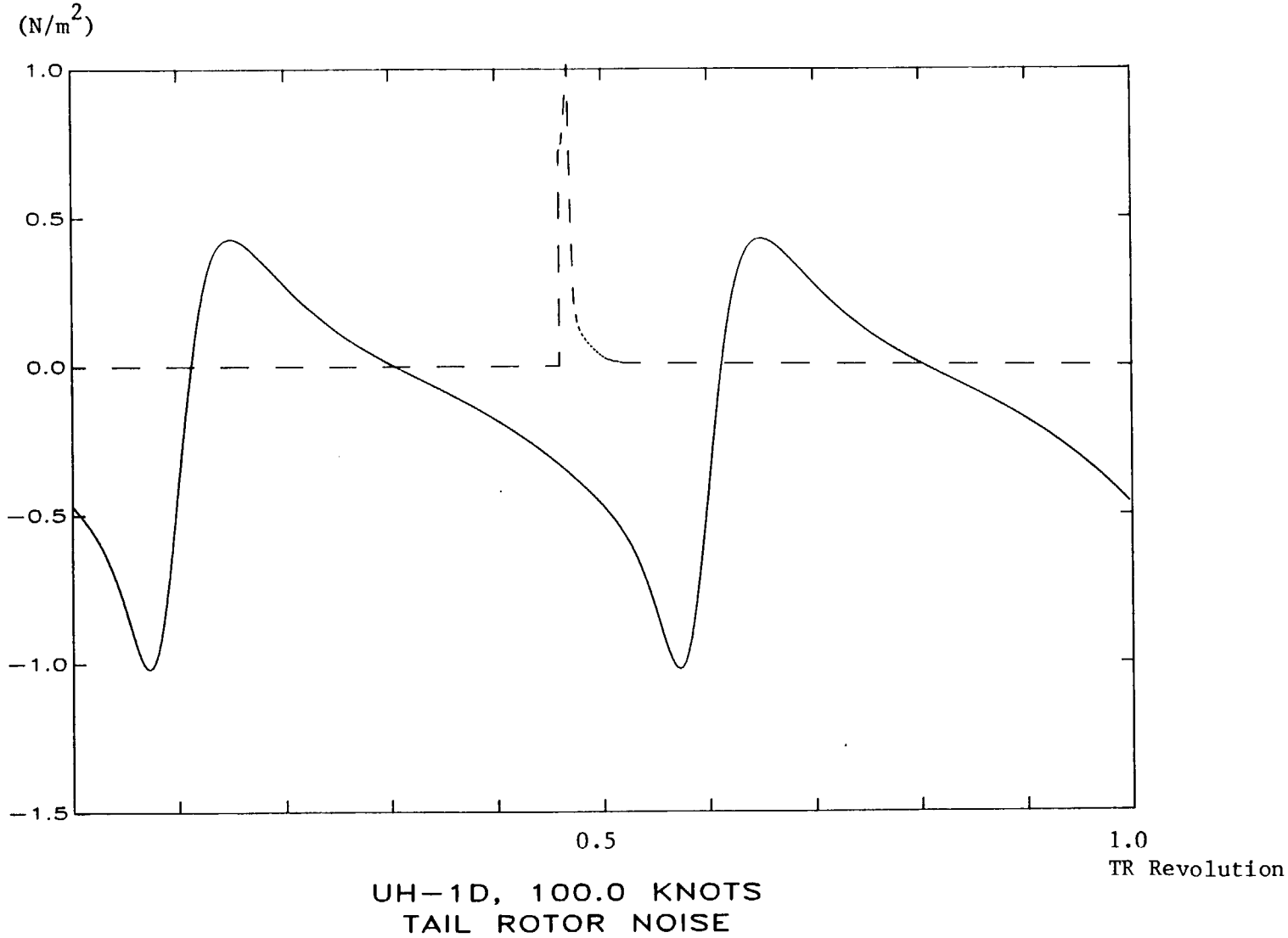

Figure 24 Comparison of Tail Rotor Blade-Vortex Interaction Noise with Thickness/ Loading Noise

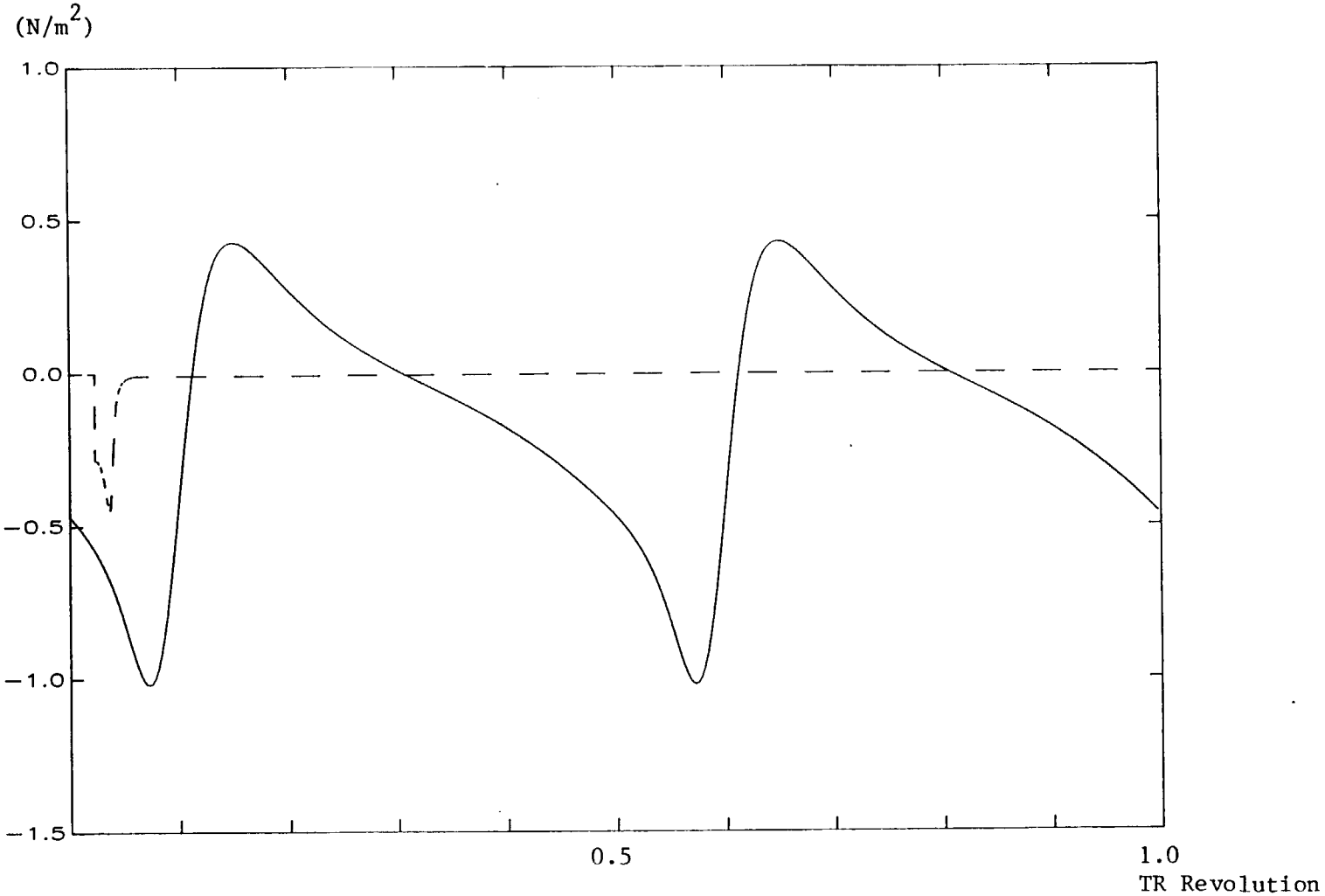

Figure 25 Comparison of Tail Rotor Blade-Vortex Interaction Noise with Thickness/ Loading Noise

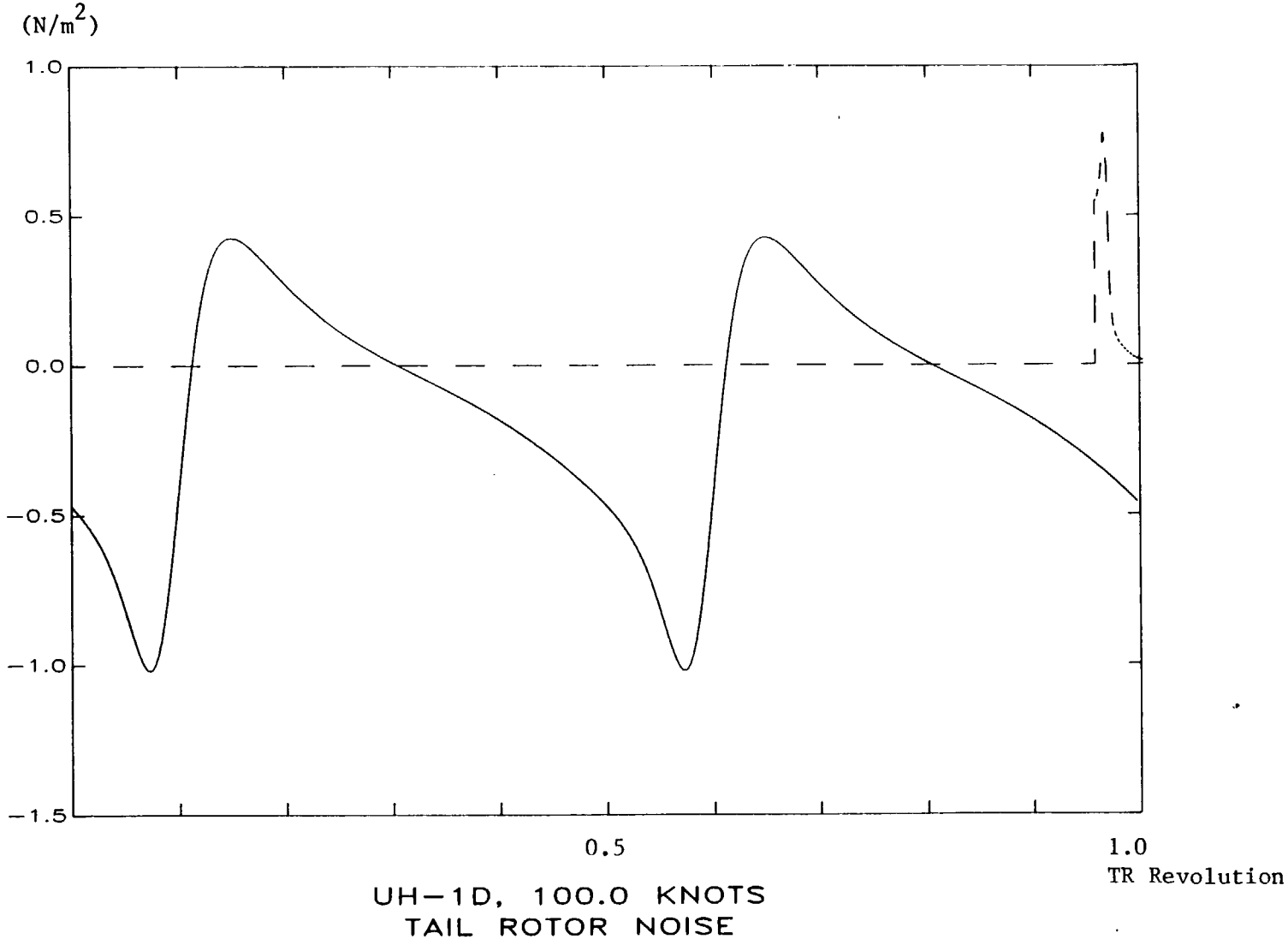

Figure 26 Comparison of Tail Rotor Blade-Vortex Interaction Noise with Thickness/ Loading Noise

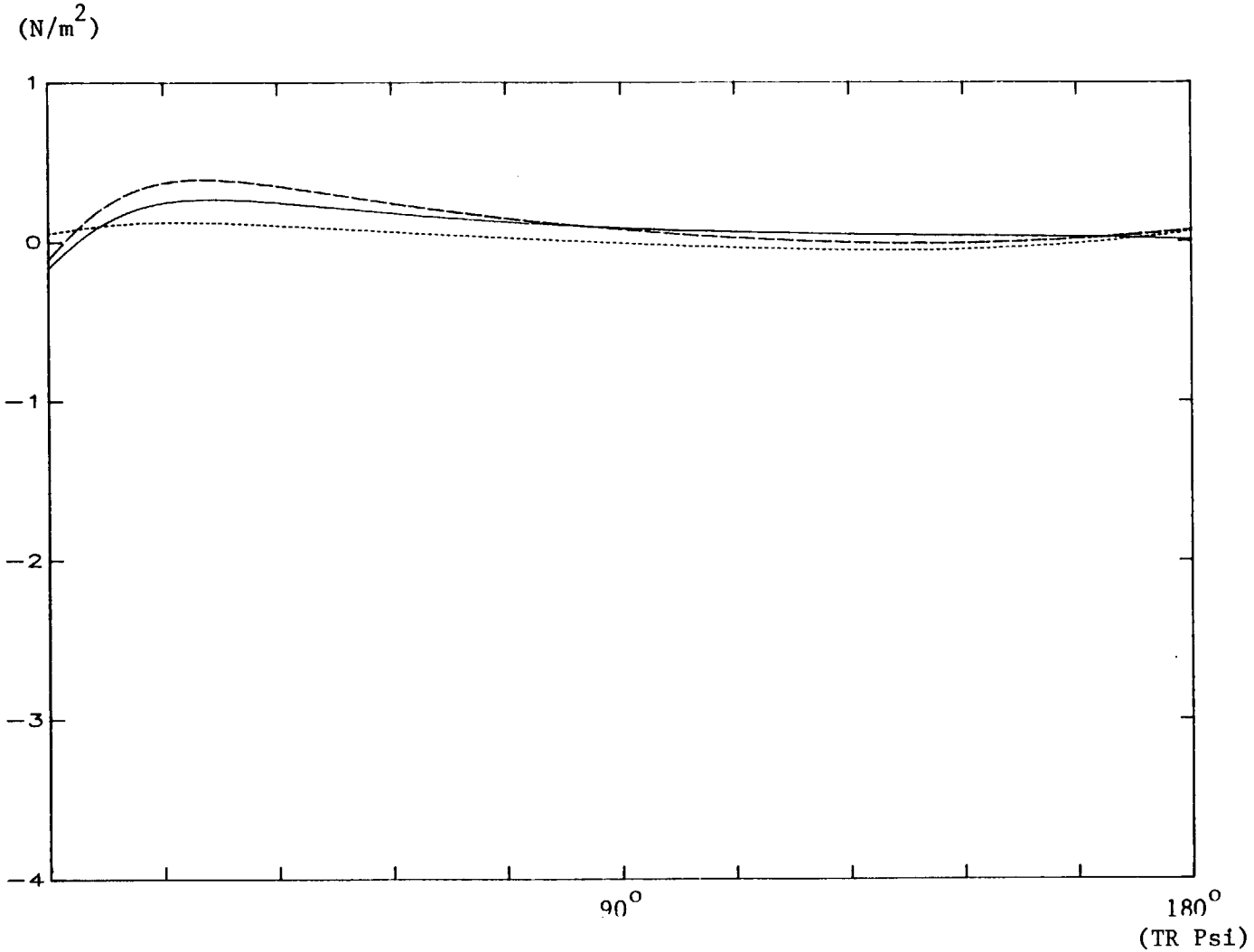

Figure 27 Tail Rotor Thickness/Loading Noise (Pressure-Time History)

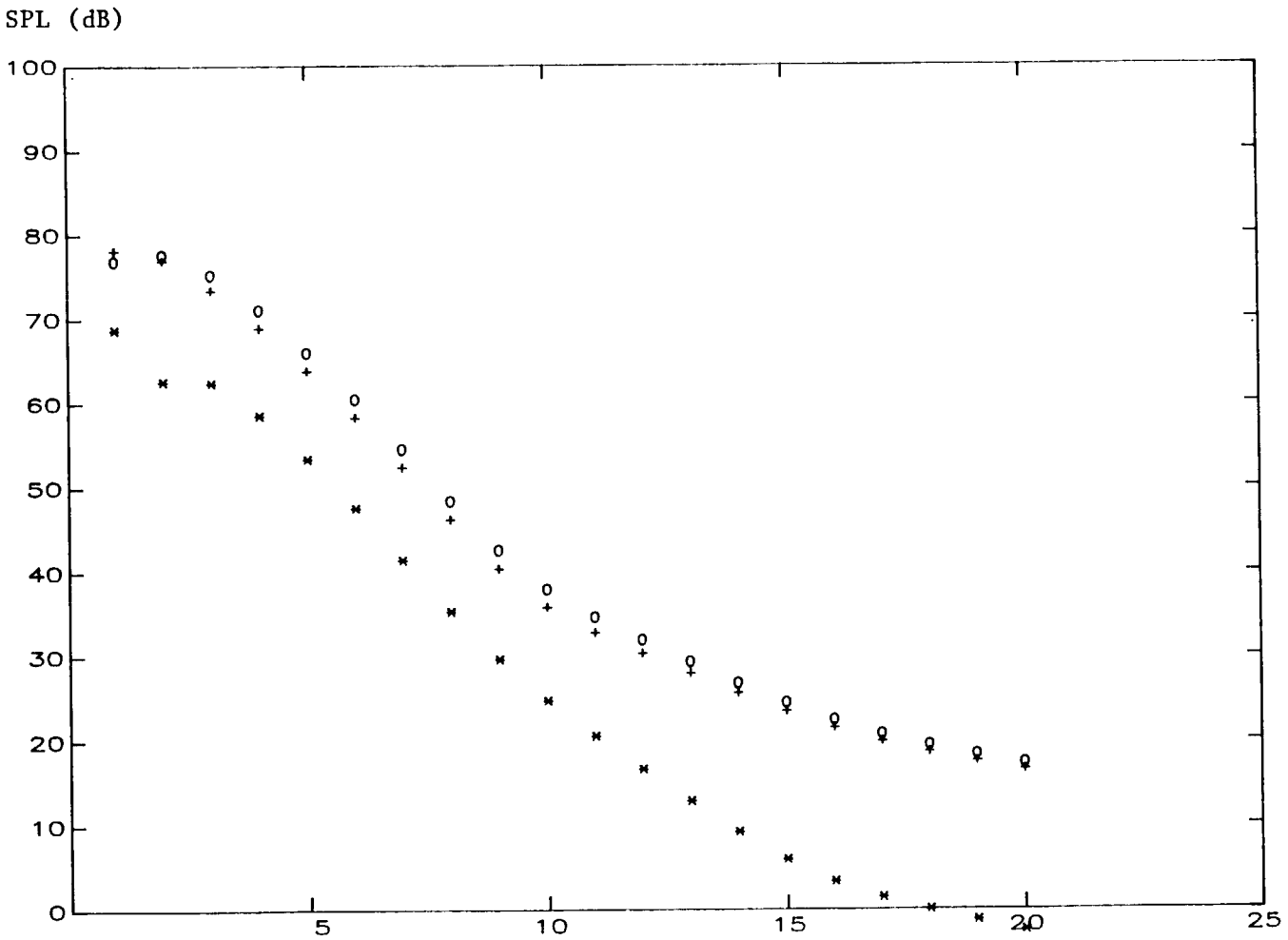

Figure 28 Tail Rotor Thickness/Loading Noise (Sound Pressure Spectrum)

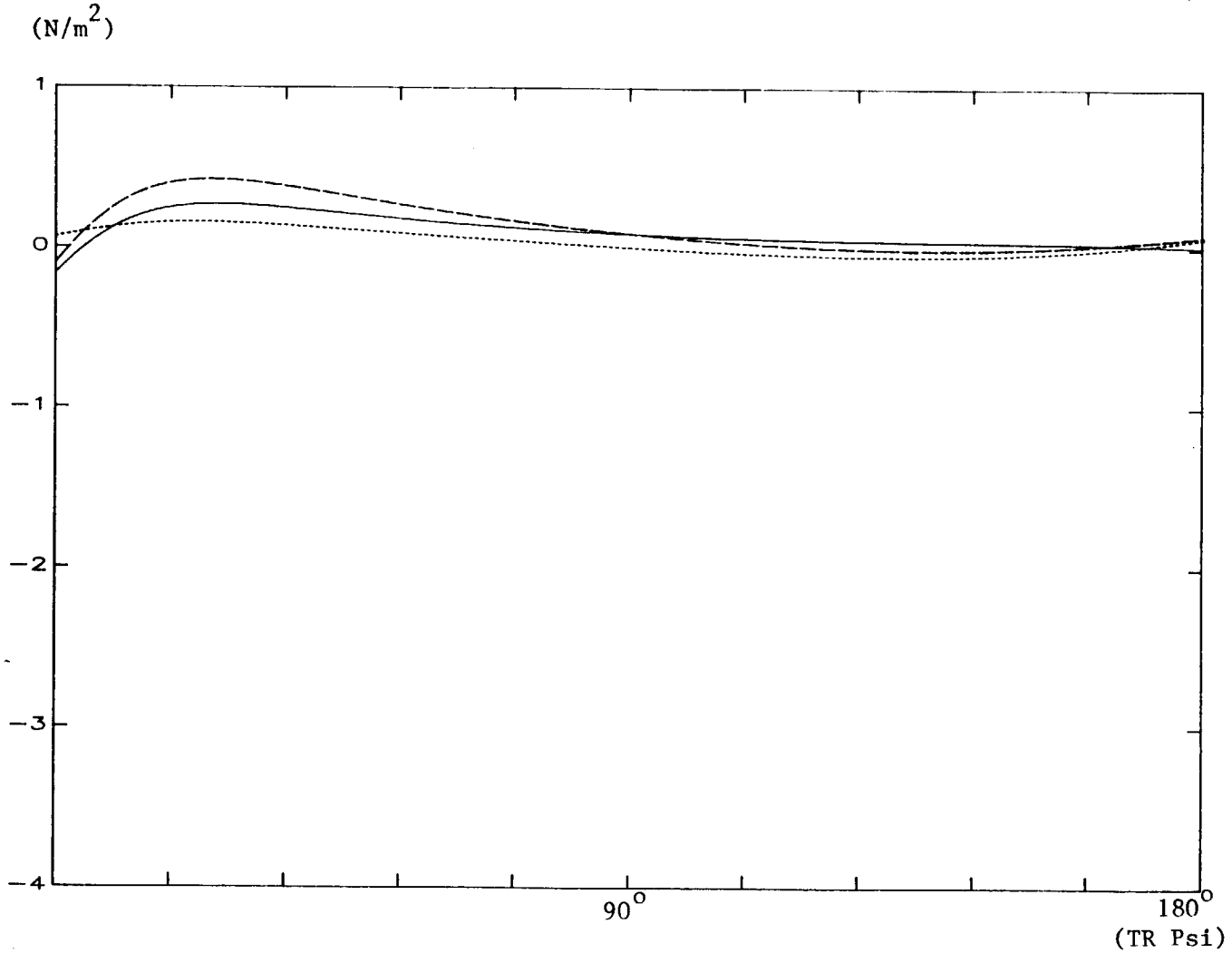

BK−117, W/O FUSELAGE WAKE

Figure 29 Tail Rotor Thickness/Loading Noise (Pressure-Time History)

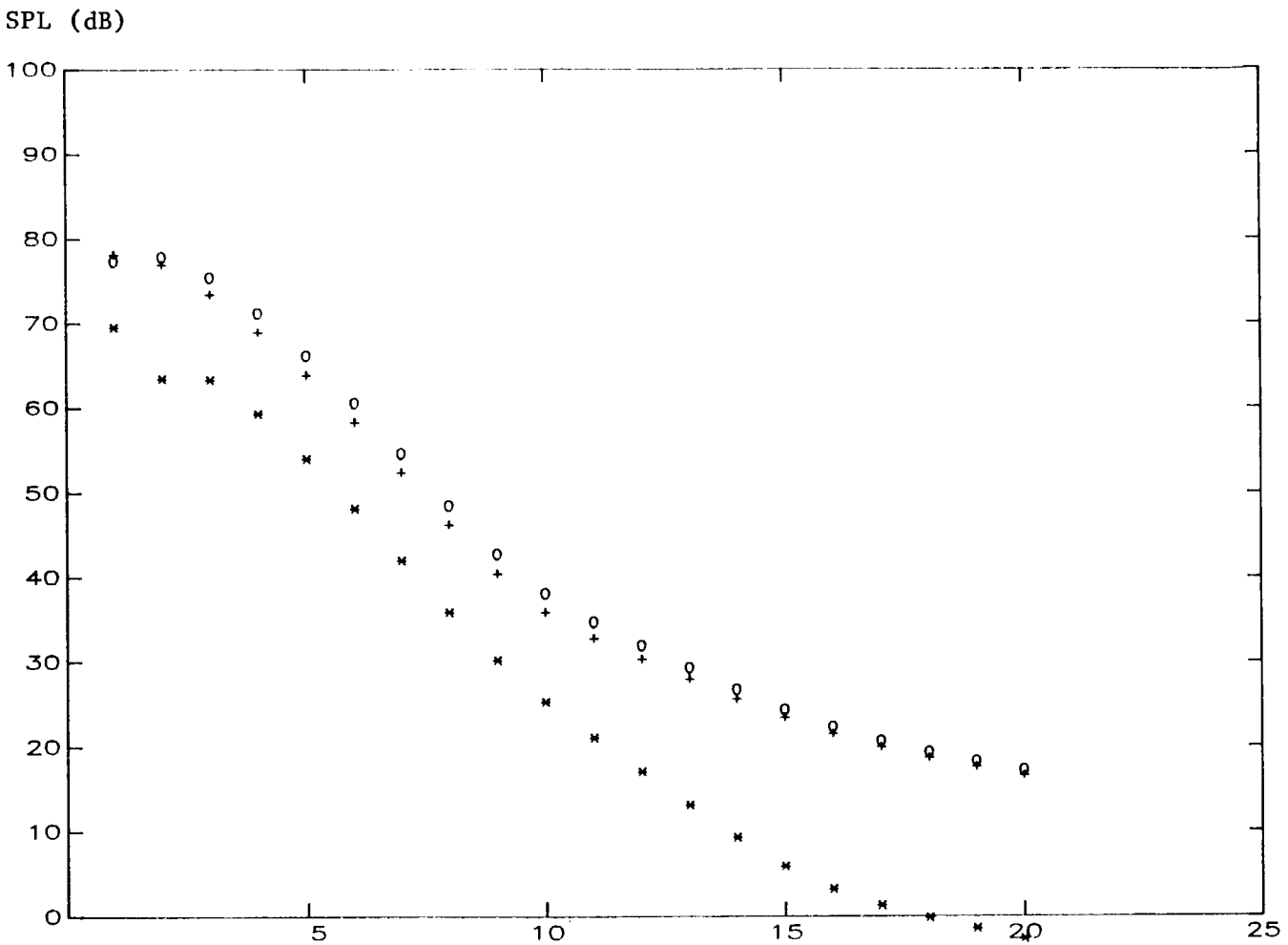

Figure 30 Tail Rotor Thickness/Loading Noise (Sound Pressure Spectrum)